NAVAL POSTGRADUATE SCHOOL

MONTEREY, CALIFORNIA

THESIS

MODELING HETEROGENEOUS CARBON NANOTUBE NETWORKS FOR PHOTOVOLTAIC APPLICATIONS USING SILVACO ATLAS SOFTWARE

by

Adam R. Garfrerick

June 2012

Thesis Advisor:	Sherif Michael
Second Reader:	Sebastian Osswald

Approved for public release; distribution is unlimited

THIS PAGE INTENTIONALLY LEFT BLANK

REPORT DOCUMENTATION PAGE			Form Approved OMB No. 0704-0188
Public reporting burden for this collection of information is estimated to average 1 hour per response, including the time for reviewing instruction, searching existing data sources, gathering and maintaining the data needed, and completing and reviewing the collection of information. Send comments regarding this burden estimate or any other aspect of this collection of information, including suggestions for reducing this burden, to Washington headquarters Services, Directorate for Information Operations and Reports, 1215 Jefferson Davis Highway, Suite 1204, Arlington, VA 22202-4302, and to the Office of Management and Budget, Paperwork Reduction Project (0704-0188) Washington DC 20503.			
1. AGENCY USE ONLY ***(Leave blank)***	**2. REPORT DATE** June 2012	**3. REPORT TYPE AND DATES COVERED** Master's Thesis	
4. TITLE AND SUBTITLE Modeling Heterogeneous Carbon Nanotube Networks for Photovoltaic Applications Using Silvaco Atlas Software		**5. FUNDING NUMBERS**	
6. AUTHOR(S) Adam R. Garfrerick			
7. PERFORMING ORGANIZATION NAME(S) AND ADDRESS(ES) Naval Postgraduate School Monterey, CA 93943-5000		**8. PERFORMING ORGANIZATION REPORT NUMBER**	
9. SPONSORING /MONITORING AGENCY NAME(S) AND ADDRESS(ES) N/A		**10. SPONSORING/MONITORING AGENCY REPORT NUMBER**	
11. SUPPLEMENTARY NOTES The views expressed in this thesis are those of the author and do not reflect the official policy or position of the Department of Defense or the U.S. Government. IRB Protocol number: N/A.			
12a. DISTRIBUTION / AVAILABILITY STATEMENT Approved for public release; distribution is unlimited		**12b. DISTRIBUTION CODE** A	

13. ABSTRACT (maximum 200 words)

Recent developments in carbon nanotube technology have allowed for semi-transparent electrodes to be created which can possibly improve the efficiency of solar cells. A method for simulating the use of semi-transparent carbon nanotube networks as a charge collector for solar cells in Silvaco ATLAS software is presented in this thesis. Semi-transparent carbon nanotube networks allow for a greater area of charge collection on the surface of solar cells as well as a lower resistance path for charge carriers to travel to the top contact grid lines. These properties can decrease the required area of a solar cell covered by metal contacts, allowing a greater amount of light input. The metal contacts which transport charge carriers to the edge of the device can also be made thicker and more spread out, lowering the resistance in the metal gridlines of solar cells.

The model for semi-transparent carbon nanotube networks presented in this thesis is incorporated into a solar cell which is simulated in Silvaco ATLAS software. The performance of a cell with and without the carbon nanotube network is compared, taking into account the limitations of the simulation software.

14. SUBJECT TERMS Carbon Nanotubes, Solar Cells, Photovoltaics, Transparent Contact, Silvaco ATLAS™			**15. NUMBER OF PAGES** 97
			16. PRICE CODE
17. SECURITY CLASSIFICATION OF REPORT Unclassified	**18. SECURITY CLASSIFICATION OF THIS PAGE** Unclassified	**19. SECURITY CLASSIFICATION OF ABSTRACT** Unclassified	**20. LIMITATION OF ABSTRACT** UU

NSN 7540-01-280-5500 Standard Form 298 (Rev. 2-89)

Prescribed by ANSI Std. 239-18

THIS PAGE INTENTIONALLY LEFT BLANK

Approved for public release; distribution is unlimited

MODELING HETEROGENEOUS CARBON NANOTUBE NETWORKS FOR PHOTOVOLTAIC APPLICATIONS USING SILVACO ATLAS SOFTWARE

Adam R. Garfrerick
Ensign, United States Navy
B.S., United States Naval Academy, 2011

Submitted in partial fulfillment of the
requirements for the degree of

MASTER OF SCIENCE IN ELECTRICAL ENGINEERING

from the

NAVAL POSTGRADUATE SCHOOL
June 2012

Author: Adam R. Garfrerick

Approved by: Sherif Michael
Thesis Advisor

Sebastian Osswald
Second Reader

Clark Robertson
Chair, Department of Electrical and
Computer Engineering

THIS PAGE INTENTIONALLY LEFT BLANK

ABSTRACT

Recent developments in carbon nanotube technology have allowed for semi-transparent electrodes to be created which can possibly improve the efficiency of solar cells. A method for simulating the use of semi-transparent carbon nanotube networks as a charge collector for solar cells in Silvaco ATLAS software is presented in this thesis. Semi-transparent carbon nanotube networks allow for a greater area of charge collection on the surface of solar cells as well as a lower resistance path for charge carriers to travel to the top contact grid lines. These properties can decrease the required area of a solar cell covered by metal contacts, allowing a greater amount of light input. The metal contacts which transport charge carriers to the edge of the device can also be made thicker and more spread out, lowering the resistance in the metal gridlines of solar cells.

The model for semi-transparent carbon nanotube networks presented in this thesis is incorporated into a solar cell which is simulated in Silvaco ATLAS software. The performance of a cell with and without the carbon nanotube network is compared, taking into account the limitations of the simulation software.

THIS PAGE INTENTIONALLY LEFT BLANK

TABLE OF CONTENTS

LIST OF FIGURES

THIS PAGE INTENTIONALLY LEFT BLANK

LIST OF TABLES

THIS PAGE INTENTIONALLY LEFT BLANK

LIST OF ACRONYMS AND ABBREVIATIONS

CNT	Carbon Nanotube
GaAs	Gallium Arsenide
I-V	Current-Voltage
I_{sc}	Short Circuit Current
V_{oc}	Open Circuit Voltage
P_{max}	Maximum Power Point
V_{max}	Maximum Power Voltage
I_{max}	Maximum Power Current
GaInP	Gallium Indium Phosphide
Ge	Germanium
SWCNT	Single-Walled Carbon Nanotube
MWCNT	Multi-Walled Carbon Nanotube
PET	Polyethylene Terephthalate
4H-SiC	4-H Silicon Carbide
AlGaAs	Aluminum Gallium Arsenide

THIS PAGE INTENTIONALLY LEFT BLANK

EXECUTIVE SUMMARY

The purpose of this thesis was to develop a working model for heterogeneous carbon nanotube (CNT) networks for use in solar cell applications while also showing the possible benefit of the use of CNTs in solar cells. Heterogeneous CNT networks are arrays of randomly oriented CNTs which have net electrical and optical properties based on the density of the network. Recent research has shown the ability to create semi-transparent CNT networks for use as charge collectors.

Heterogeneous CNT networks were modeled as completely transparent, low band gap semiconductor materials with sheet resistances based on experimental data from recent research in heterogeneous CNT networks. To account for the optical properties of the CNT network models created, the input power spectrum of light was altered in solar cell simulations which included a CNT layer. The spectrum was multiplied by a series of scale factors which are based on recent research on the optical properties of CNT networks. The resultant input power was designed to be equivalent to the light input power that would be seen by the solar cell under a thin CNT layer.

Two CNT network models of different sheet resistance values were used as a top conducting layer in a Gallium Arsenide (GaAs) solar cell while placing a gold contact on the top of the cell. A GaAs solar cell and the two cells including CNT networks were simulated in an experiment which gradually increased solar cell width while keeping the gold contact width constant. This experiment compared the performance of the solar cells while the distance photogenerated charge carriers had to travel to the contact increased.

The simulations showed that as the cell width reached relatively large values, the GaAs cell had significant degradation in its maximum power point based on voltage losses due to charge carriers travelling to the top contact via semiconductor materials in the solar cell. The two solar cells with CNT layers did not show this degredation as the generated charge carriers had a low resistance path to the top contact through the heterogeneous CNT layer.

The results of this thesis show that heterogeneous CNT networks can improve the performance of solar cells with relatively large distances between top contacts. Though the CNT model created in this thesis includes many simplifications and assumptions, it serves as a functional baseline for the modeling of heterogeneous CNT networks. This model can easily be modified to more accurately match the behavior of CNT networks, leading to the design and optimization of highly efficient solar cells including heterogeneous CNT networks.

ACKNOWLEDGMENTS

I would first like to thank my thesis advisor Dr. Sherif Michael for his guidance and direction on my thesis work. I would also like to acknowledge Matthew Porter for his help with all issues regarding Silvaco ATLAS incurred throughout my research.

I would finally like to thank my parents who have always been supportive and put an emphasis on my education. Their support and encouragement were a great help through this process.

THIS PAGE INTENTIONALLY LEFT BLANK

I. INTRODUCTION

Solar cells are semiconductor devices that transfer light into usable electrical power. These devices were originally studied as early as 1839 by Antoine-Cesar Becquerel who noticed that light shone on diodes induced an electrical current. However, a relatively efficient solar cell generating a reasonable amount of power was not created until 1954 when Chapin, Fuller, and Pearson developed a silicon based solar cell for Bell Labs. Since the creation of the first viable solar cell, research regarding the technology and the improvement of the efficiency of solar cells has rapidly increased. The recent emphasis on the use of renewable energy and the desire for power in remote areas such as space has put this research further into the forefront.

One of the most promising areas of research in the improvement of solar cell efficiency is the use of carbon nanotubes (CNTs) in solar cells. Heterogeneous networks of CNTs have recently been shown to have the ability to act as a semi-transparent conductor[1]. This capability is optimal for use in solar cells as electrical contacts or as a method for reducing the percentage of a cell covered by metal contacts. The metal contacts on a solar cell block input light that could be converted into power. Because CNTs can possibly reduce the coverage of metal contacts on a solar cell and have greater conductivity than semiconductor materials, they have the ability to improve the efficiency of solar cells.

Sumio Ijima is often credited with the discovery of CNTs[2]. His research spurred investigation in the physics community which proved that CNTs had remarkable structural and electrical properties that could be used in many applications. Most notably, CNTs were found to have maximum current densities two to three times greater than metals commonly used as conductors. More recent research has shown that CNTs can be deposited onto materials in random arrays to create a heterogeneous conducting network which only absorbs and reflects a small portion of the light shined upon it based on the density of tubes in the network[6]. This discovery has led to much research in the solar cell community regarding the use of CNTs as transparent conducting layers.

The goal of this thesis was to model a heterogeneous CNT network in Silvaco ATLAS software and use the model to show the possible benefits of the use of CNT networks as a surface layer in all solar cells. The model created was based on recent experimental data on heterogeneous CNT networks. This model was used as the top layer of a Gallium Arsenide (GaAs) solar cell which was simulated in ATLAS software.

II. BACKGROUND

The use of CNTs to improve the efficiency of solar cells is investigated in this thesis. To understand how solar cells and CNTs function, a basic understanding of semiconductor physics is required. The fundamental principles of semiconductor physics and solar cells are reviewed in this chapter.

A. SEMICONDUCTOR BASICS

Semiconductors are materials which can act either as an electrical insulator or conductor based on the conditions in which they operate. This behavior is due to the bonding properties of the individual atoms that form a bulk material and the interactions between their outer electrons. The individual atoms of semiconductors, like all other atoms, have a set structure that determines how they will bond with other atoms.

1. Atomic Structure and Quantum Theory

An individual atom consists of positively charged protons, neutrons with no charge, and negatively charged electrons. It is held together by the attractive forces of the oppositely charged protons and electrons. The structure of an atom consists of a central nucleus composed of protons and neutrons that is orbited by a cloud of electrons. This electron cloud is made up of quantized shells that have an associated energy level. Every electron in this orbiting cloud must reside at a quantized energy level. An electron can move to a higher energy shell by absorbing energy or drop to a lower shell by releasing energy. This arrangement of electrons in the quantized shells is the most important determining factor in an atom's interactions with other atoms and, therefore, its electrical properties.

In every atom, each electron has a unique set of quantum numbers which describe its energy state in the atom. The four quantum numbers are represented by the letters *n*, *l*, *m*, and *s*. The first number *n* represents the shell that the electron occupies. Higher shell levels have electrons in higher energy states than lower shell levels. The *l* and *m* numbers denote subshells that appear within each shell and each can hold two electrons of

opposite spin. The *s* number represents the spin of the electron and can either be a positive or negative value. The possible values of each of the quantum numbers are summarized in Table 1.

Table 1. The possible values of all possible quantum numbers are given

Quantum Number	**Possible Quantum Number Values**
n	n=(1, 2, 3, …, n) where n corresponds to the energy level of the outermost shell
l	l=(0, 1, 2, …, $n-1$)
m	m=($-l$, $-l+1$, …, $l-1$, l)
s	s=($-1/2$, $+1/2$)

2. The Crystal Lattice

Every solid material is made up of individual atoms organized in a certain manner and can be classified as amorphous, crystalline, or polycrystalline based on their arrangement. The basic lattice structure of amorphous, crystalline, and polycrystalline materials are shown in Figure 1. The most abundant solids found naturally on the earth are usually amorphous, meaning their individual atoms have no ordered arrangement. Contrastingly, a crystalline material is a material that has a periodic arrangement of atoms, called a crystal lattice, which is repeated throughout the solid. Therefore, the solid appears the same when examined at the atomic level at any point. Materials that do not fall into either the amorphous or crystalline category are classified as polycrystalline. These materials are composed of different regions which each have a periodic arrangement of atoms, but the whole material is not uniform in its arrangement.

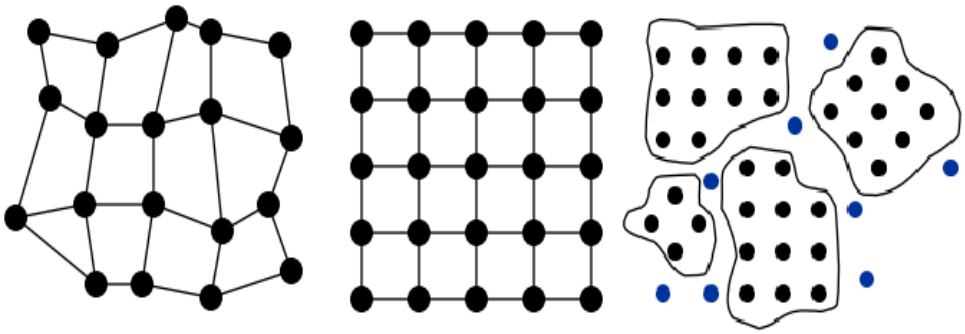

Figure 1. Figures 1(a), 1(b), and 1(c) show the atomic structures for amorphous, crystalline, and polycrystalline materials, respectively. After [2]

Crystalline solids, which are the most commonly used materials in solar cell applications, can be further classified based on the type of structure of their crystal lattice. Every lattice can be reduced to a unit cell, a small volume which is representative of the whole cell. This unit cell forms a geometry which can take many forms. The most common forms are the variations of the cubic and diamond lattices. An example of a diamond crystal lattice is given in Figure 2. A material can be thought of as a large object composed of large quantities of these unit cells put together as building blocks.

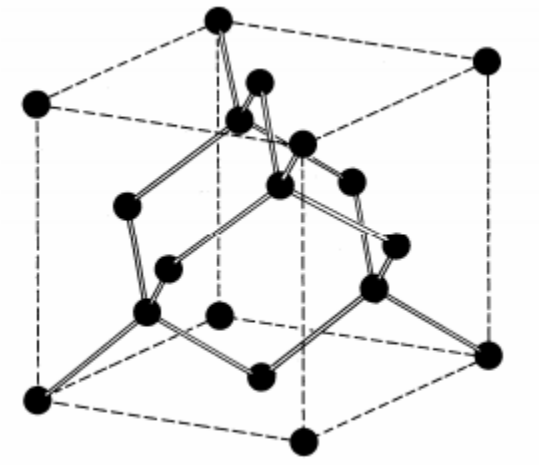

Figure 2. The diamond lattice is shown with each black dot representing an individual atom and each solid line representing a bond between atoms. After [2]

A semiconductor material's unit cell structure determines many of its important properties in solar and electrical applications. The numbers and types of bonds between atoms of the material determine the characteristics of the flow of charge carriers in the material, defining parameters such as resistivity and conductance. The arrangement of the atoms also determines whether certain materials can be grown in layers adjacent to one another to create a certain device. If two material lattice structures do not match in a certain manner, lattice mismatch will occur, a condition in which the lattices of two adjacent materials cannot create an appropriate electrical interface due to conflicting lattice structures. These properties governed by the crystal lattice combine with the properties and structure of the individual atoms to give every material unique properties.

3. Energy Bands

In much the same way that electrons can only reside at certain quantized energy levels in an individual atom, they are restricted to inhabiting energy bands in a solid. However, each of these energy bands is made up of a range of energy levels which each electron can occupy. This difference arises from the influence of all neighboring atoms on an electron. In the case of an individual atom, an electron resides in a quantized shell with an associated energy level. If two atoms are close enough to each other, their electrons and other attractive forces will influence each other, creating different energy states in specific bands of energy. In the band diagram in Figure 3, interatomic distance is graphed against electron energy. The band diagram shows that when atoms of the same element are infinitely far away from each other, they have the same quantized energy levels. However, when the atoms are closer together, the electrons of each atom interact, and the discrete energy levels diverge into a band of allowed energies shown by the grey portion of the graph in Figure 3.

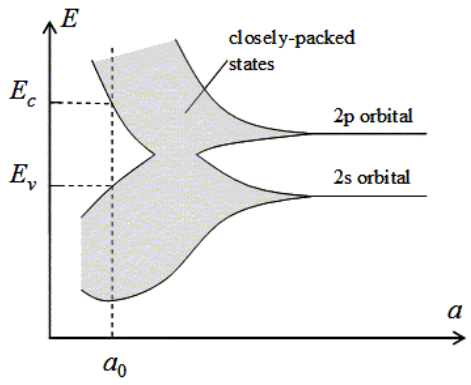

Figure 3. Inter-atomic distance is graphed against energy to show the formation of energy bands in a material. From [3]

The only energy bands of major concern in solar cell applications are the valence band and the conduction band. The valence band is the outermost energy shell of each atom. The electrons in this band are usually held in place by bonds between atoms. If an electron in the valence band receives energy greater than or equal to the difference in energy in the conduction and valence band, known as the bandgap, then it will move into the conduction band. When it moves into the conduction band, the electron breaks away from its bond and becomes a free electron in the material. An electron can only move up to the conduction when gaining energy in the valence band because there are no allowable energy states for an electron to occupy within the bandgap.

A material's ability to conduct electricity is highly dependent on its bandgap. Insulators have a relatively large bandgap and take a large amount of energy to excite free electrons. Semiconductors have a relatively small bandgap, allowing them to act as an insulating or conducting material dependent on the level of energy in the material. Conductors have overlapping valence and conduction bands and, therefore, have free charge carriers without the addition of outside energy. The differences in bandgap among insulators, semiconductors, and conductors are shown in Figure 4. The bandgap decreases as conduction ability increases.

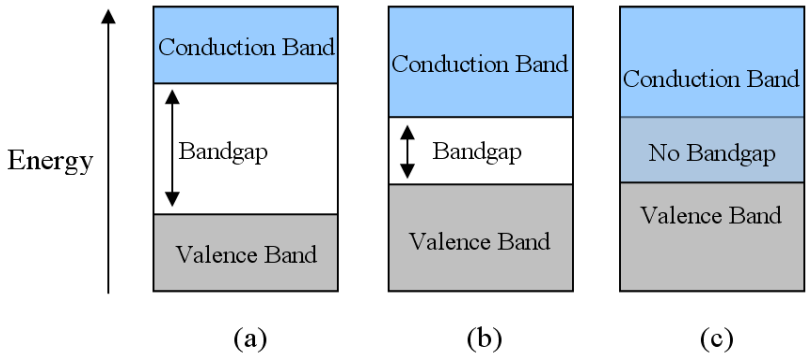

Figure 4. The relative bandgaps of insulators, semiconductors, and conductors are shown in Figures 4(a), 4(b), and 4(c), respectively. From [4]

Semiconductors have a moderate bandgap due to the unique conditions in their valence bands. All elemental or single element semiconductors have four electrons in the valence band of each atom. These elements are known as group IV elements. The atoms of these materials bond with each other to fill the outer shell of each of the surrounding atoms by the use of four covalent bonds with neighboring atoms. These covalent bonds can be broken by the introduction of energy, which frees charge carriers. Other semiconductors are made up of compounds in which the two element's valence electrons sum to eight. This can be achieved in many different elemental combinations to create effective semiconductor materials.

4. Charge Carries

When bonds are broken in a material due to the absorption of energy, two different types of charge carriers are created called electrons and holes. Electrons are simply the negatively charged elements of atoms and are considered free electrons when they break away from a bond. Holes are conversely the positive charge left behind by the broken bond of the free electron. Unlike free electrons, holes exist in the valence band. Holes are not physical particles but are merely positive charges created by the lack of necessary electrons for charge balance. Though holes are not physical particles with a mass, their flow is associated with a positive value of current while electron flow is associated with negative current.

Electrons and holes each have an associated mobility in every material based on how easily the free charge carriers can move through the material. Though electrons and holes are of equal charge, electrons have a higher mobility. A material's electron and hole mobility are dependent on many material characteristics such as the lattice structure, the size of the atoms in the material, and the orientation of the channel in which the charge carrier is travelling. The electron and hole mobility determine parameters such as the conductance and resistivity of a material, which are important factors in solar cells.

5. Doping

Doping is the process of purposefully introducing impurities into a semiconductor material for the purpose of manipulating its electrical characteristics. A pure, undoped semiconductor is called intrinsic, while a doped semiconductor is called extrinsic. A semiconductor can be doped with either *p* or *n* type material. The *p* type dopants, called acceptors, have three or less valence electrons. This type of dopant bonds with all the surrounding atoms but lacks enough electrons to fully fill its outer shell. Thus, it attracts electrons, inducing the generation of holes in the material. An *n* type dopant, known as a donor, has five or more valence electrons, allowing it to fully bond with all of the neighboring atoms while leaving an extra, unbonded electron. This electron can easily be excited into the conduction band because it is not bound by the energy of a covalent bond. The extra charge carriers created by doping can greatly increase charge carrier concentrations, allowing for the fabrication of materials more suited to most applications than intrinsic semiconductors.

6. The P-N Junction

Most of the applications of semiconductors, including solar cells, are possible due to the properties created by the junction between a *p*-type region and an n-type region. The region where these two materials meet is called a *p*-*n* junction and functions as a diode. In this region, excess electrons in the *n* region and excess holes in the *p* region diffuse across the border of the two regions to form a depletion region in which oppositely charged ions create a barrier that blocks charge flow. The formation of the depletion region from the junction of *p*-type and *n*-type materials is shown in Figure 5.

The instant the materials meet, the excess carriers of each material border region move to the other material, attracted by the holes or electrons on the other side of the junction. These charges leave behind ions that then have a negative charge in the case of the *p* side and a positive charge in the case of the *n* side. This barrier then blocks charge flow because the electrons on the *n* side are repelled by the negative region on the edge of the *n* side and the opposite is true of the holes on the *p* side. If the junction is forward biased with a voltage greater than the potential of the depletion region potential, then the diode conducts current. If the diode is reversed biased, it acts as an insulator and the depletion region expands.

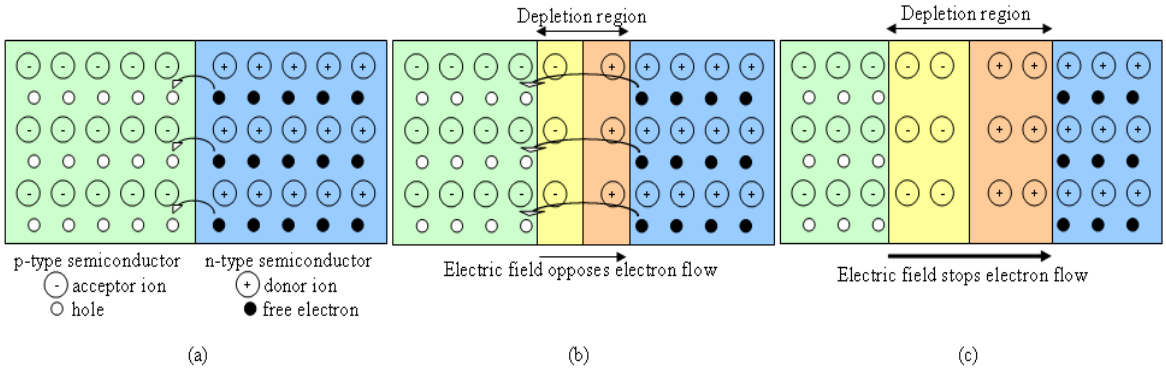

Figure 5. The junction between an *n*-doped and *p*-doped material forms a depletion region. Figure 5(a) shows majority carriers travelling across the junction due to the attraction caused by opposite charge carriers. The barrier caused by newly formed ions is shown in Figures 5(b) and 5(c). From [4]

B. SOLAR CELL OPERATION

Due to the properties of the *p*-*n* junction and the ability of semiconductors to absorb energy via photons of light, solar cells are able to generate power. The basic concepts behind solar power and the important characteristics which can quantify a solar cells performance are explained in this section.

1. Origin of Solar Power

A basic solar cell consists of a *p*-*n* junction with metal contacts on both sides of the junction. In an *n* on *p* solar cell the top *n* layer is called the emitter, while the bottom *p* side is called the base. When placed in an environment with light, the solar cell absorbs

photons which generate electron hole pairs near the depletion region. To generate power, the metal contacts to the emitter and base are tied together via an external load as shown in Figure 6. Due to the field of the depletion region, charge carries generated by photons are swept across the depletion region so that a photocurrent is generated in the reverse biased direction. However, when an external load is applied, the current induces a voltage across the load. This voltage induces a countering forward biased current that is less than the photocurrent but increases as the load reaches infinity. The net current in a solar cell is always in the reverse biased direction but decreases as the forward biased current increases with an increasing load. The power produced by the cell is the product of the net current and voltage across the load.

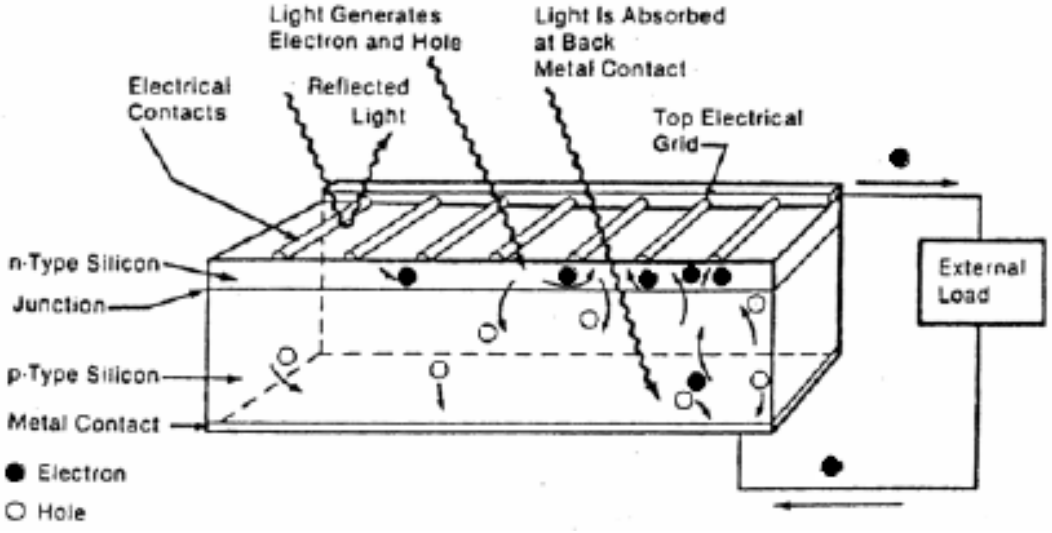

Figure 6. Power is delivered to an external load from a simple *n* on *p* solar cell (arrows denote electron flow). From [5]

2. Solar Cell Characteristics

The most useful characteristic of a solar cell is its current-voltage (I-V) curve. This curve graphs the solar cell's net current per unit surface area in the *y* direction against the associated load voltage in the *x* direction. A typical solar cell I-V curve is shown in Figure 7, which shows anode voltage plotted against cathode current. As discussed in the previous section, the value of load resistance affects both the load voltage and net current generated in the solar cell. The *y* intercept of the I-V curve is the

limiting case in which there is no load resistance and a maximum value of current called the short circuit current (I_{sc}) occurs. In this case there is no induced voltage across the load, creating no forward biased current to counter the photon induced current. The *x* intercept represents the extreme case in which the load resistance is infinite, producing a maximum voltage known as the open circuit voltage (V_{oc}). In this case no current can flow due to the infinite resistance. Opposing charges are built up on both sides of the depletion region of the *p*-*n* junction, resulting in a maximum voltage across the infinite load. Though it is useful to know I_{sc} and V_{oc} for a solar cell, it is more useful to know the the maximum power point (P_{max}). The maximum power current (I_{max}) and voltage (V_{max}) can then be determined. These values show the actual power capability of a solar cell, the most important factor in the cell's application. The parameters V_{oc}, I_{sc}, I_{max}, and V_{max} are shown in Figure 7 on an I-V curve.

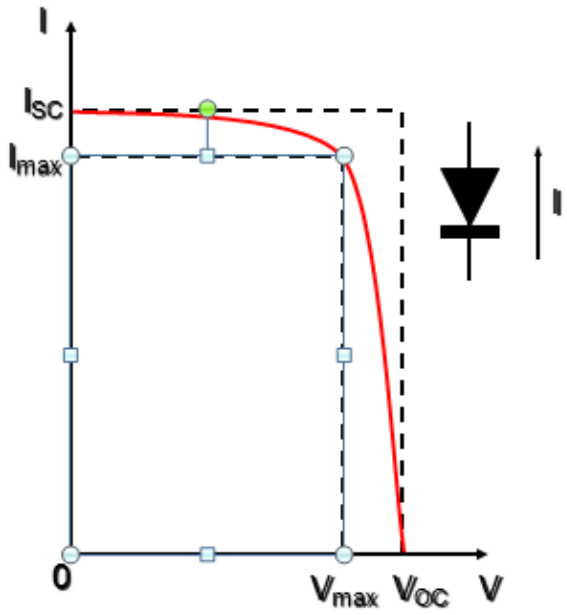

Figure 7. The typical I-V curve for a solar cell which graphs anode voltage against cathode current is shown. V_{oc}, I_{sc}, I_{max}, and V_{max} are shown to display the limiting cases of the I-V curve and the maximum power point. From [6]

Once the I-V curve for a solar cell is determined, many parameters can be calculated which are useful in comparing the performance of different cells. Solar cell efficiency η is given by

$$\eta = \frac{P_{max}}{P_{in}} \times 100\% \quad (1)$$

where P_{max} is the maximum achievable power of the solar cell and P_{in} is the input power from the light applied to the cell. The fill factor *FF* is given by

$$FF = \frac{P_{max}}{V_{oc} I_{sc}} \quad (2)$$

where V_{oc} and I_{sc} are the open circuit voltage and short circuit current, respectively. The *FF* is a measure of how well a solar cell transfers its short circuit current and open circuit voltage properties into actual power. These two parameters are useful for comparing solar cells but are dependent upon the input power to the solar cell, which varies based upon the light source applied.

3. Solar Cell Input Power

The input power to a solar cell is dependent upon the light source in which the cell is operating. In this thesis, air mass zero (*am0*), the ambient light in space, is used. The *am0* spectrum has different power values depending on distance from the sun. The *am0* spectrum at Earth orbit and Martian orbit as well as the spectrum of light at the Martian surface are shown in Figure 8. As expected, greater distance from the sun and transmittance through an atmosphere cause drops in power levels. The power level seen while orbiting the earth is 136.7 mW/cm^2. This power is delivered over a range of wavelengths with the net power being the integrated power spectrum.

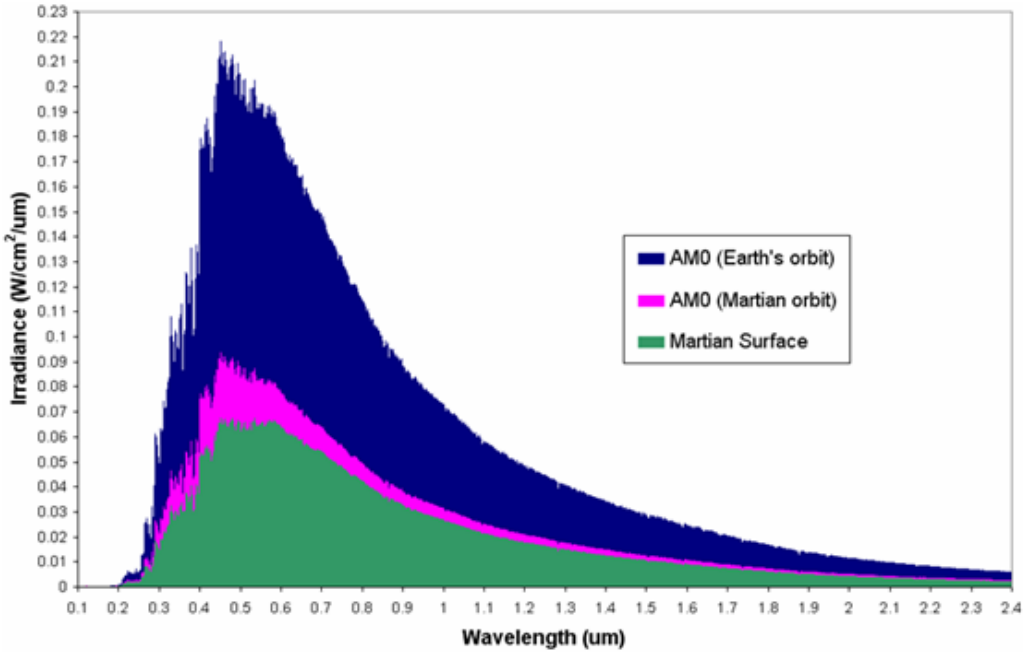

Figure 8. The *am0* spectrum is shown for Earth orbit, Martian orbit, and the Martian surface. From[6]

Due to the properties of solar cells, only part of the solar spectrum can be converted into electrical power. This is caused by the different bandgaps and optical properties of materials. The bandgap of a material determines the minimum amount of energy required to generate an electron hole pair in the material. Any photon with energy less than the bandgap will simply pass through the material without exciting an electron. The energy of a photon is dependent on its wavelength and is given by

$$E = \frac{1.24}{\lambda} \tag{3}$$

where E is in units of eV and λ is the wavelength of the photon in μm. The shorter the wavelength of a photon, the higher its energy and ability to generate electron hole pairs in higher band gap materials.

Though it would seem that lower band gap materials would have the ability to harness the widest range of photons, photons with energies much greater than the band gap of a material are not very efficient at generating electron hole pairs. To easily display

a solar cell's response to photon energy, a spectral response curve graphs photon wavelength against the efficiency of charge carrier generation. The spectral response of three different commonly used solar cell materials is given in Figure 9. Different materials have different curves that are limited to a maximum wavelength based on the material band gap and a threshold at which photons have too much energy. In this thesis the mid-level band gap material gallium arsenide (GaAs) is used. GaAs has a spectral response which indicates efficient charge carrier generation by photons ranging in wavelength from 0.6µm to 0.9µm as seen in Figure 9.

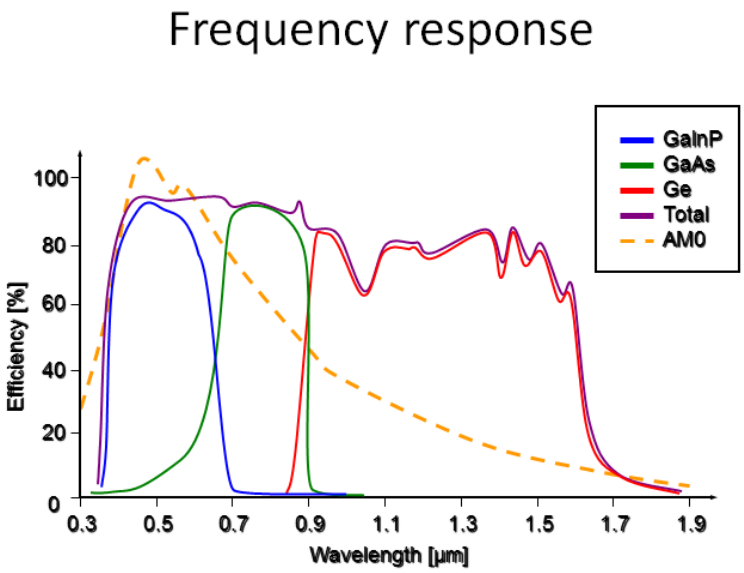

Figure 9. The spectral responses of gallium indium phosphide (GaInP), gallium arsenide (GaAs), and germanium (Ge) solar cells are graphed along with the *am0* spectrum. From [6]

4. Solar Cell Performance

Though solar cell performance is largely dominated by a material's spectral response and I-V characteristics, there are many other factors that influence a solar cell's performance. The more important factors that affect solar cell performance are:

- The reflection of light off the surface of a solar cell limits the amount of input power into the cell. The optical properties of different materials cause a portion of the photons hitting the solar cell to be reflected off the surface. This can cause a

35% loss in the theoretical efficiency of a solar cell without the use of antireflective techniques[6].

- Photons with energy much higher than the band gap generate electron hole pairs, but the excess energy is dissipated as heat in the crystal lattice of the solar cell. Low energy photons that do not generate charge carriers also bombard the atoms in the crystal lattice and create heat. This heating causes a loss in the voltage of a solar cell. A solar cell loses 2mV/K in voltage, which can drastically lower the efficiency of a solar cell[6].
- Recombination of electrons and holes can cause the charge carriers generated by photons to meet in the lattice and cancel each other out. When this happens a free electron meets with a hole in the valence band and occupies that space, no longer contributing to the number of charge carriers in the solar cell[6].
- Material defects in the solar cell can create traps which create more recombination. Cheaper, less pure materials can have significant defects that negate much of the generated current[6].
- The resistance of the bulk material causes a voltage drop within the solar cell that reduces the efficiency. When charge carriers are generated, they have to travel to the contacts of the solar cell to be harnessed as energy. The distance travelled through the lattice is often relatively great for each charge carrier, creating a high resistance seen by each of the charge carriers. This decreases the net voltage seen at the contacts[6].
- Shading from the top electrical contact completely blocks light to portions of the solar cell. The optimal top contact grid usually covers 8% of a solar cell. This 8% of the solar cell surface receives no photons to generate charge carriers and does not contribute to the power production of the solar cell[5].

The problems of internal resistance and shading in solar cells are addressed in this thesis through the use of carbon nanotubes (CNTs). With a net reduction in the resistance seen by each of the charge carriers and a reduction in the percentage of the solar cell surface covered by the top contact, the efficiency of any solar cell can be increased. The

improved conductivity on the surface of a solar cell that could be provided by a CNT layer could increase the distance between metal grid lines which collect current. These lines could, therefore, be made thicker, reducing losses from resistance in the grid lines, further increasing the efficiency of a solar cell.

C. CHAPTER SUMMARY

The background in semiconductor physics and solar cells necessary to understand the research in this thesis was provided in this chapter. The basic properties of semiconductors were shown to be optimal for generating solar power. The ability to generate electron hole pairs by the absorption of photons with energy greater than the bandgap allows solar cells to deliver power to a load. The producible power was shown to be dependent on both the material of the solar cell and the spectrum of input light. The power was also shown to be limited by factors inherent in the real properties of fabricated solar cells.

The structure and properties of CNTs is covered in the next chapter to provide the basic knowledge necessary in understanding photovoltaic CNT applications.

THIS PAGE INTENTIONALLY LEFT BLANK

III. CARBON NANOTUBES

As their name implies, CNTs are carbon based tubes on the nanometer scale that have a variety of useful properties. These tubes were first discovered in 1991 by Sumio Iijima as an odd structure of carbon atoms[7]. Later research on these structures revealed both semiconducting and metallic electrical properties based on their structure, allowing for a variety of useful applications. Metallic CNTs have been shown to have current density capabilities two to three times greater in magnitude than commonly used metals[8]. The additional relation of CNT tube diameter and structure to the bandgap of semiconducting CNTs can lead to semiconducting materials with a controllable bandgap[9]. The use of CNTs as a semi-transparent charge collector to improve solar cell performance is the focus of this thesis. Therefore, a basic understanding of the structural and electrical properties of CNTs is necessary.

A. CARBON NANOTUBE STRUCTURE

The basic building block of CNTs is the carbon atom. A carbon atom has six electrons. Like all other elemental semiconductors, four of a carbon atom's electrons are valence electrons. To form a CNT, carbon atoms can be thought of as first arranging as a material called graphene. Graphene is structured as a hexagonal arrangement of carbon atoms in a single sheet called a honeycomb lattice which is shown in Figure 10. This sheet of graphene has many useful conductive properties but is more importantly the basis for the formation of CNTs.

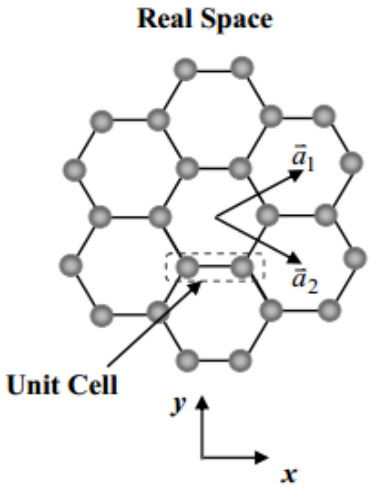

Figure 10. The Crystal lattice of graphene is shown. From [2]

Though the process of forming CNTs is more complicated, it can be thought of as rolling a sheet of graphene and placing hemispheric carbon based caps on both of the tube ends. Based upon the orientation of the rolling of the graphene sheet, CNTs can take on either semiconducting or metallic properties. An example of a semiconducting and metallic CNT is shown in Figure 11. Though the visualization of a simple roll of graphene aids in the understanding of CNTs, the structural properties and methods of CNT formation are much more complex.

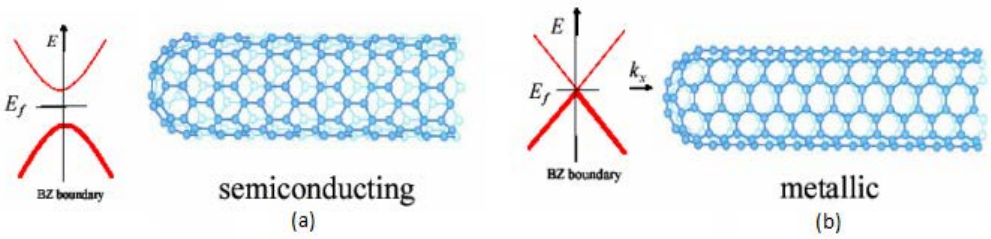

Figure 11. A semiconductor CNT (a) and metallic CNT (b) are shown with their associated band diagrams. After [2]

The most pertinent quantities defining CNTs are the characteristics of the CNT's chiral vector C_h. The chiral vector C_h is a vector in the unrolled CNT's honeycomb lattice defined as

$$C_h = na_1 + ma_2 \equiv (n, m) \tag{4}$$

where n and m are integers and a_1 and a_2 are the lattice defining vectors of graphene shown in Figure 12. The values of n and m determine the length L of C_h, which is the circumference of the CNT, and the chiral angle θ. The chiral angle is the angle between the chiral vector (n, m) and the zigzag direction of the honeycomb lattice (n, 0)[9]. These two properties are integral in defining a CNT's electrical characteristics. Certain combinations of L and θ give semiconductor characteristics, while others induce metallic characteristics.

The unit cell of a CNT is the rectangular region bounded by the chiral vector C_h and the vector T, which is shown in Figure 12. The vector T is the one-dimensional translation vector of the CNT that extends from the origin of the C_h vector to the first lattice point **B** in the honeycomb lattice, which is shown in Figure 12[9]. In more simplified terms, the point **B** is the first carbon atom in the honeycomb lattice that is intersected by the line propagating in the normal direction to C_h. The vector T is defined similarly to C_h as

$$T = t_1a_1 + t_2a_2 \equiv (t_1, t_2) \tag{5}$$

where t_1 and t_2 are integers.

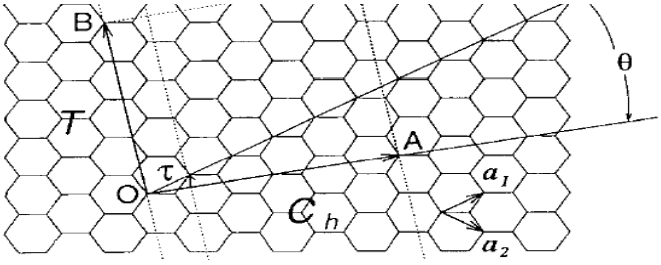

Figure 12. The unrolled honeycomb lattice of a CNT is shown. The chiral vector C_h which is composed of the lattice vectors a_1 and a_2 is shown along with the T translational vector. The symbol Θ is the chiral angle, while the point B represents the first point at which T intersects a carbon atom in the honeycomb lattice. From [9]

Based on the properties of their C_h and T vectors, CNTs can be divided into one of three structural categories known as armchair, zigzag, and chiral, which are shown in Figure 13. A CNT falls into these three categories based on its chiral angle θ, which can vary from zero to thirty degrees. At the boundaries of θ, zigzag CNTs have a chiral angle of zero degrees, while armchair CNTs have a chiral angle of thirty degrees. Chiral CNTs have a chiral angle that lies anywhere between but not including zero and thirty degrees[9].

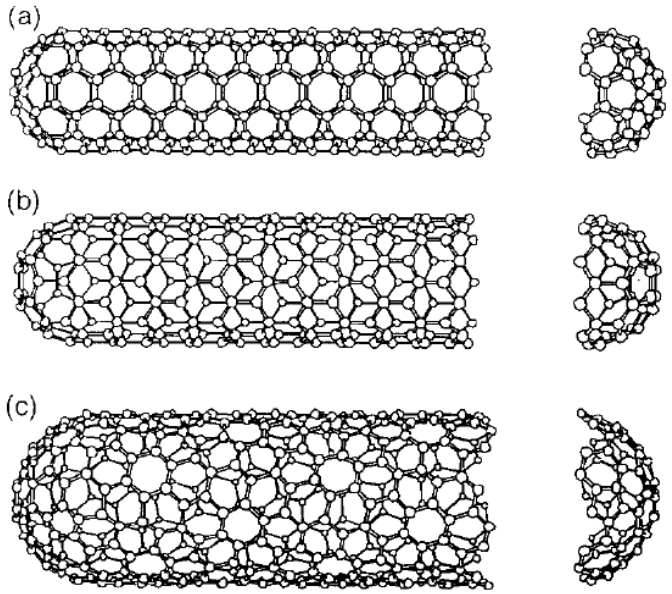

Figure 13. Armchair (a), zigzag (b), and chiral (c) CNTs are shown. From [9]

There are many more structural qualities which define CNTs, but these are more complex than the basic understanding required for this thesis. The basic structural properties discussed in this section are the properties that govern each individual CNT's physical properties. These properties determine how a CNT will act in electrical applications.

B. CNT PROPERTIES AND POSSIBLE SOLAR CELL APPLICATIONS

CNTs come in two forms when actually grown, single-walled carbon nanotubes (SWCNTs) and multi-walled carbon nanotubes (MWCNTs). SWCNTs are structured with one layer of graphene rolled into a CNT. MWCNTs are contrastingly composed of

multiple layers of graphene rolled in the same manner. The focus of this thesis is on heterogeneous networks of SWCNTs as transparent conductors, which, when grown, produce a variety of semiconducting and metallic nanotubes[10]. Due to the somewhat random distribution of CNTs formed in heterogeneous networks, one third of the tubes are metallic, and the others semiconducting[9]. All of the possible CNTs that can be formed from graphene's honeycomb lattice are shown in Figure 14. Because the metallic nanotubes are highly conductive, they dominate the electrical characteristics of the layer of CNTs.

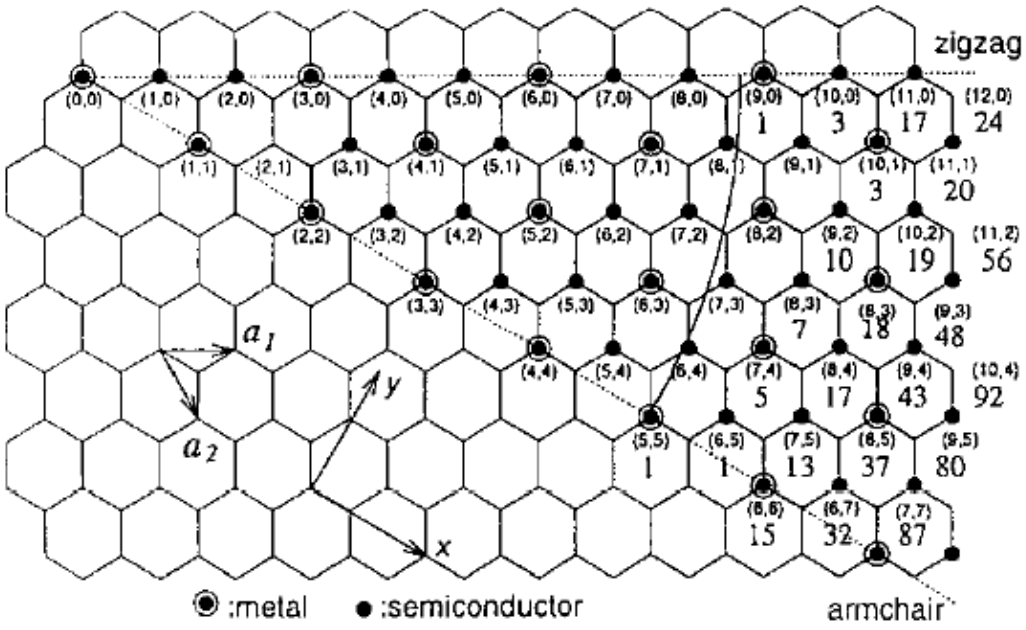

Figure 14. All possible orientations of CNTs are shown in which a third are metallic and all others are semiconducting[9]

The conductance and sheet resistance of heterogeneous networks of CNTs have been simulated by the *Stick Percolation Model* and verified by experimental data in recent research[10]. This model, which represents the CNT network as an area of randomly distributed, conducting and semiconducting sticks, aids in the understanding of charge flow in a CNT network. Two examples of simulations of the stick percolation model are shown in Figure 15. In this model, a two-dimensional area is randomly populated with conducting and semiconducting sticks with random orientation. Since the

model simplifies the problem of charge flow in a network of highly complex structures, it is solvable by drift diffusion theory[10]. This model gives a useful visual representation of a heterogeneous network. A layer of CNTs on the top layer of a solar cell has the same random orientation of conductors that have a net conductance based on the density of conducting tubes in the area. Higher densities of conducting tubes allow for higher conductance values.

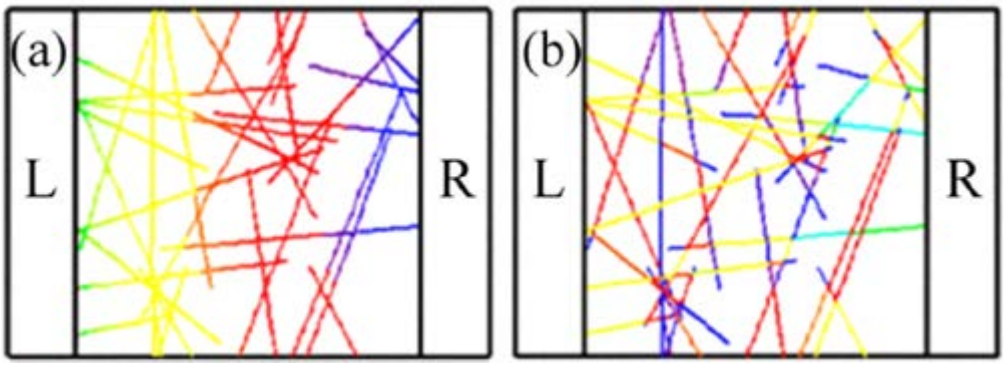

Figure 15. Two examples of simulations of the stick percolation models of CNTs are shown where L and R are electrodes and the different colored sticks represent CNTs. The area between the electrodes was randomly populated with CNTs and the resistance across the region was calculated. After [10]

One reason for the prominence of CNTs in solar cell research is the ability to make layers of them semitransparent to have a larger area of charge collection while lowering the effect of shadowing from solar cell contacts. One of the primary methods for depositing heterogeneous CNT networks onto the surface of solar cells involves dipping the cells into a solution with a variable density of CNTs and baking the network onto the surface[1]. In depositing a heterogeneous CNT network onto the surface of a solar cell, the level of transparency can be controlled by the density of CNTs in the depositing solution. The experimental spectral response of two different CNT density electrodes is shown in Figure 16. The electrode with lower sheet resistance was dipped into the CNT solution twice to give a higher CNT density in the electrode. The higher density solution has a lower sheet resistance but also a lower percentage of light transmittance.

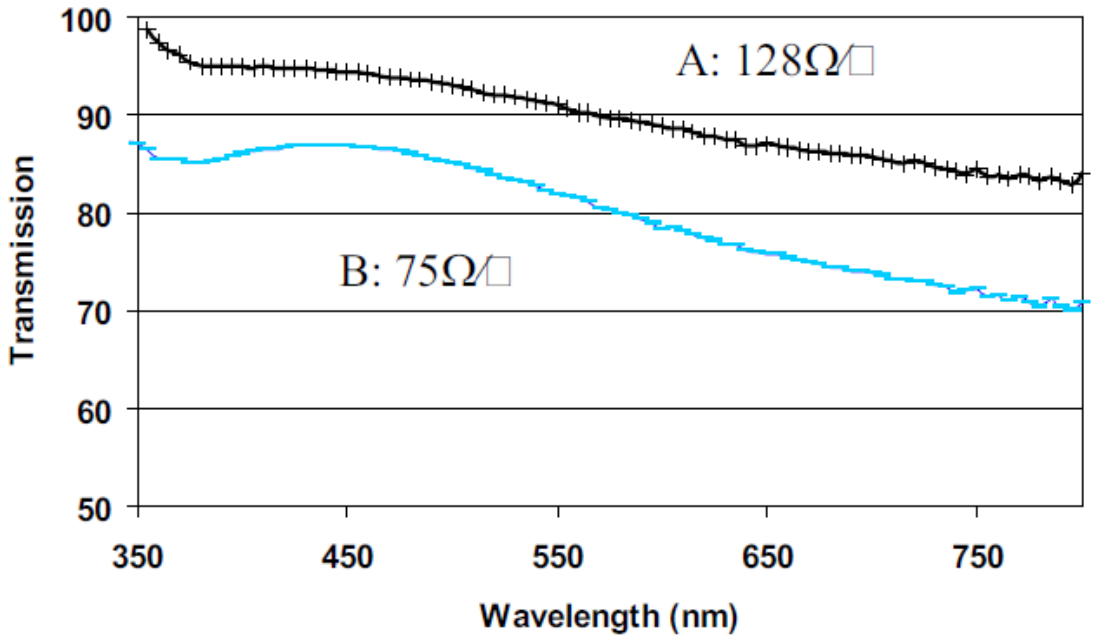

Figure 16. The spectral response of two different semi-transparent CNT films is plotted as wavelength against transmittance percentage. From [1]

C. CHAPTER SUMMARY

The basic structural and physical properties of CNTs were covered in this chapter. CNTs can be thought of as tubes of rolled graphene that can take on either semiconducting or metallic properties based on the orientation in which they are rolled. Heterogeneous networks of these tubes, which are the subject of this thesis, are areas randomly populated by CNTs. These networks have a net conductance and light transmittance based on the density of CNTs in the area. The ability of CNT networks to have high conductance while being semitransparent makes them optimal for use in solar cells.

Solar cell modeling and simulation in Silvaco ATLAS software is covered in the next chapter. This program was used to simulate solar cells with a CNT layer in this thesis.

THIS PAGE INTENTIONALLY LEFT BLANK

IV. SOLAR CELL MODELING

The modeling of solar cells using the ATLAS device simulator, which is a part of the TCAD software package, is a focus of this thesis. An overview of how ATLAS simulates device behavior and how this is applied to solar cells is given in this chapter.

A. DEFINING A STRUCTURE IN THE ATLAS DEVICE SIMULATOR

The ATLAS device simulator, by Silvaco International, is a computer program which uses solid state physics and numerical analysis to simulate the behavior and characteristics of electrical devices. The software takes a two-dimensional input structure which is specified and gridded by the user through an input program and solves the differential equations derived from Maxwell's laws to simulate the transport of carriers within the structure at each of the points of the grid. The user can specify any type of device using a large library of conductors, semiconductors, and insulators and can use solve statements to simulate the behavior of a device under certain conditions. The text input deck, Deckbuild, is used for the specification and solve statements of devices in this thesis. In Deckbuild, users type input commands that first specify the structure and then set the conditions for simulating its behavior. These statements must follow a set structure to properly run the ATLAS software. An ordered description of the types of statements and their functions gives the best understanding of the ATLAS device simulator.

1. Defining Constants

Before defining a structure to be analyzed by the ATLAS program, the user can define constants to make later structure modifications easier. The statement

```
set baseThick=0.3
```

creates a baseThick constant which can be used anywhere in the program after it is defined. The constant has to be prefaced with the "$" character whenever it is used in the later code. Constants allow the user to change one statement instead of changing each occurrence of a value in the code.

2. Defining the Mesh

The first section of structure defining statements in the Deckbuild program is the meshing section. This section specifies the two-dimensional grid that is applied to the device with mesh statements. This grid does not have to be constant throughout the structure but can have finer or coarser areas depending on the desire of the user. This is useful because areas such as *p*-*n* junctions require fine meshing due to the abrupt changes in properties across the junction. The ATLAS device simulator can more easily solve the differential equations at each grid point if there are no abrupt changes between adjacent points.

Mesh statements have two parts called location statements and spacing statements. The location statement, *loc*, specifies the *x* or *y* value in the structure to which the following spacing statement is applied. The spacing statement, *spac*, specifies the spacing between grid lines at that specific location. The ATLAS software ensures that the spacing is the stated value at the specified location but gradually increases or decreases the spacing to meet the requirement of the next spacing statement. Typical structures have coarser mesh lines at unimportant areas that converge to a finer spacing at more important areas such as *p*-*n* junctions or contact areas.

The other statement commonly used in the creation of solar cell meshing is the width statement. This statement does not affect the mesh points created but applies a scale factor to all calculations, simulating a device of the specified width. The default value for all devices in the *z* direction, which can be thought of as pointing into the computer screen, is one micron. The width factor can be used to simulate a change in this value but does not create a *z* direction mesh. The statement causes the ATLAS software to apply a scale factor to the one micron cell, essentially scaling up the results of the small device simulation. Though the width statement in Deckbuild is not explicitly meant to be used as a scale factor, it is useful for obtaining results in the right form and units and is used this way in this thesis. A typical solar cell mesh with the corresponding mesh statements is shown in Figure 17. The constants used set the locations at which a certain spacing values occur. The *width3d* constant is set to apply a scale factor to all solutions which converts currents to A/cm^2.

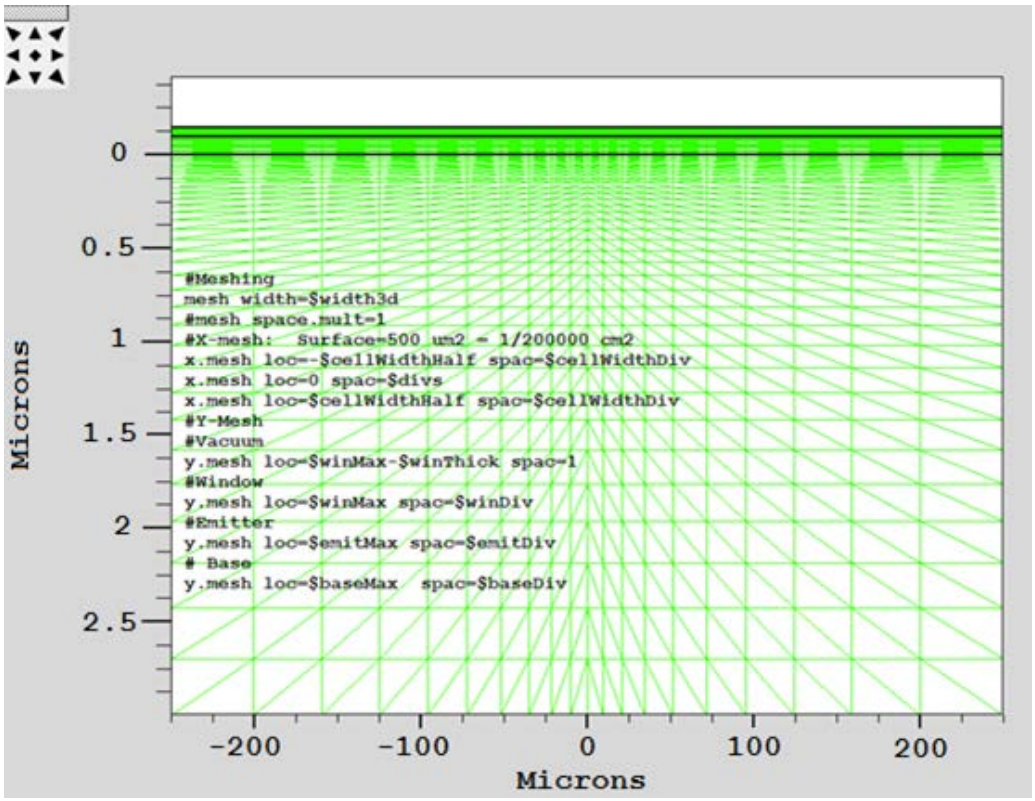

Figure 17. The mesh statements creating the mesh for a simple GaAs solar cell are displayed along with a picture of the created mesh

3. Setting the Regions

Once the meshing of a device structure is specified, the device can be divided into regions. These regions all share a number of characteristics specified by the user. Each region is composed of a specific material which has certain default parameters that can be changed by the user in the later material properties section of the code.

The region statements include a region number, a material specification, and the region boundaries. The region number is arbitrary but is used in later structure specification sections to apply characteristics to certain regions. Every region must have a different number as the program produces an error if a statement applies to two different regions. The material specification statement specifies that the whole region consists of the stated material. This statement gives that whole region default parameters and characteristics that are in the ATLAS material library. These values include material

parameters such as the bandgap, electron and hole mobility, and optical properties such as the index of refraction. These parameters may be used or changed in another section of the structure defining code if the user wishes to modify a material's properties.

The most important part of the region statement is the region boundary. A region's boundaries are set by defining maximum and minimum *x* and *y* values in the 2D grid. Using these statements, the user is limited to rectangular regions. More complicated regions can be created with other programs that run ATLAS software but were not used in this thesis. The code used to define the regions of a simple GaAs solar cell along with the corresponding visual representation of the created regions is shown in Figure 18. In this code, three different rectangular regions are created that each have specific properties defined later in the Deckbuild code.

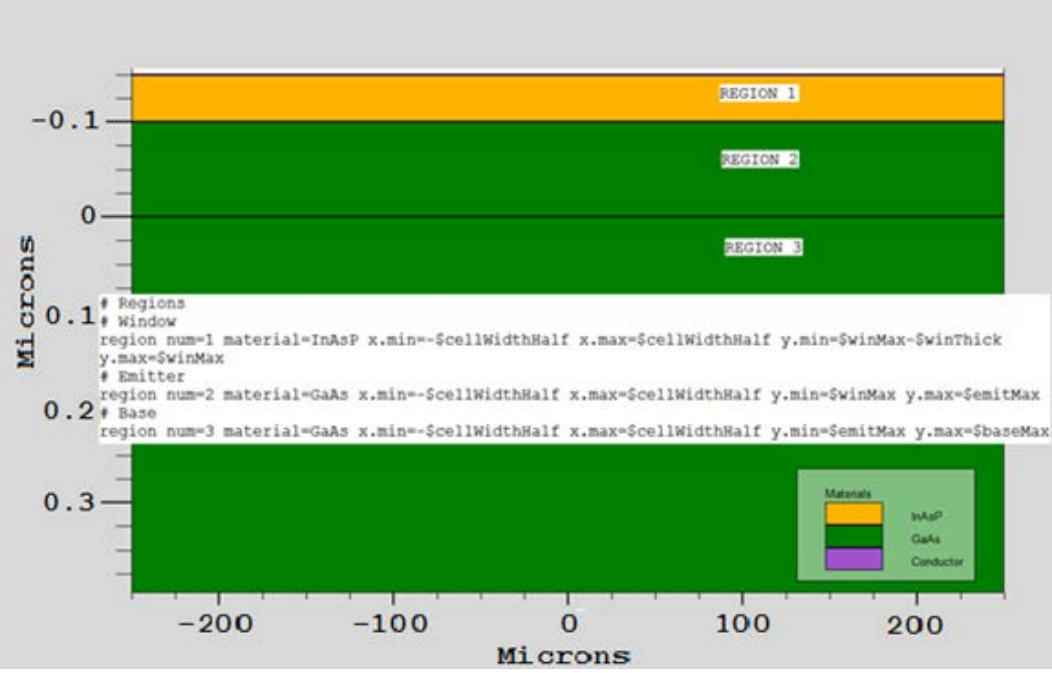

Figure 18. The Deckbuild code creating the regions of a simple GaAs solar cell is displayed along with a picture of the created regions

4. Defining Electrodes

The electrode statements of the structure defining code specify the contacts of the user's electrical device. The user has the ability to specify any number of electrodes with

different metallic properties. Each electrode declaration typically has three parts. The user must first name each electrode. The name can be followed by a material statement, which specifies the type of metal of the contact. The ATLAS material library includes many metals that have different default values which are used unless later changed. The last statement defines the boundaries of the electrode. The boundary statement uses maximum and minimum *x* and *y* values to set the boundaries of each electrode.

For solar cell modeling, it is often sufficient to only name the electrodes and specify them as covering the top and bottom of the solar cell. If this type of electrode is specified, the electrode is by default made to be a perfect conductor which absorbs no light. This condition is ideal for simulating solar cells while neglecting the effects of top contacts which complicate the simulation. A simple GaAs solar cell with transparent contacts covering the top and the bottom of the cell is shown in Figure 19 along with the corresponding Deckbuild code.

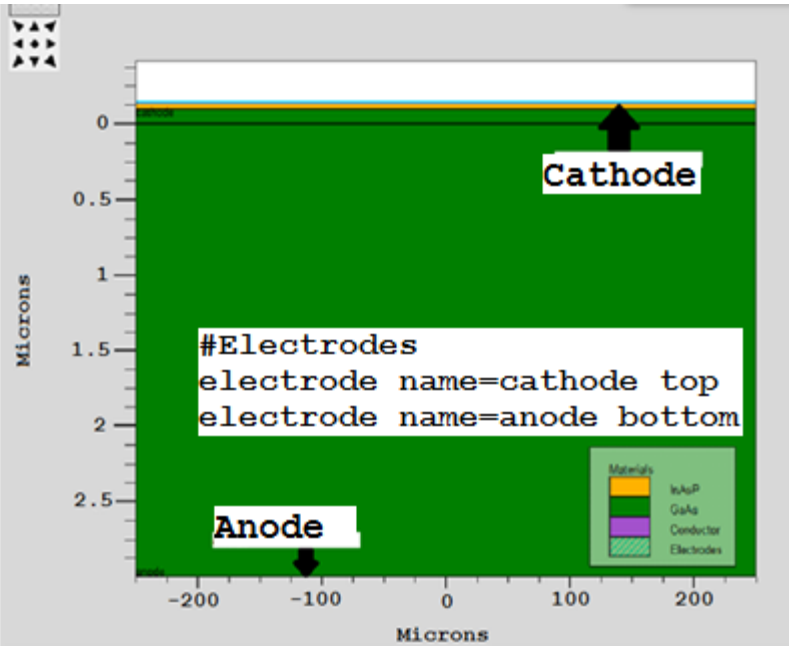

Figure 19. A GaAs solar cell with a transparent, perfectly conducting cathode and anode is shown along with the electrode defining code

If the user desires to incorporate real contacts into the solar cell, the electrode boundaries and properties can be defined. The typical electrode statement in this thesis

consists of three parts including the contact name, contact material and contact boundaries. A GaAs solar cell with a gold top contact is shown in Figure 20 along with the corresponding Deckbuild code.

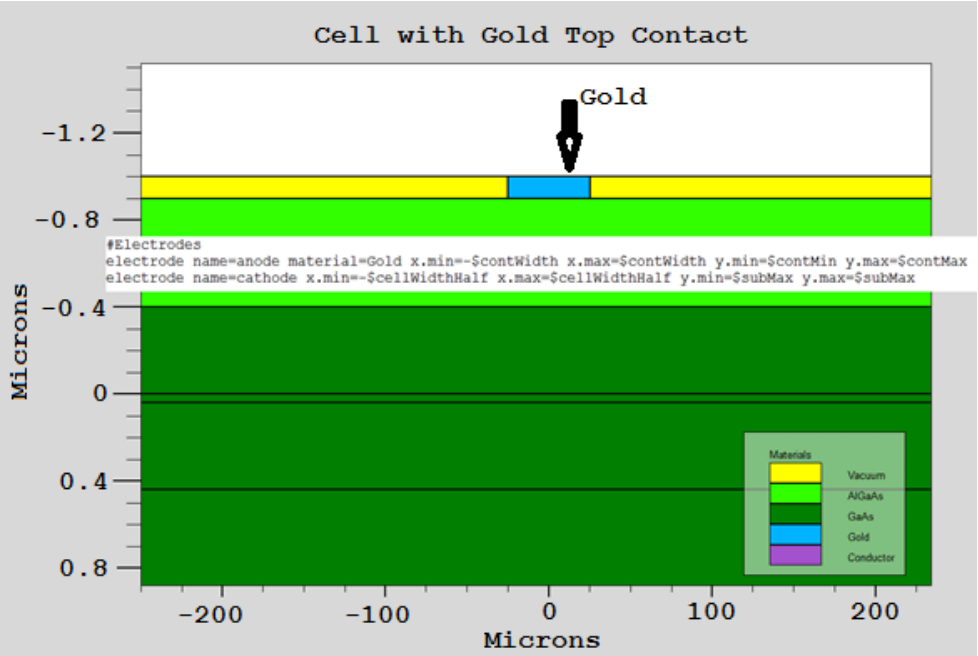

Figure 20. A GaAs solar cell with a real gold top contact is shown with the corresponding electrode statements in the Deckbuild code

5. Setting Doping Levels

The doping statements specify the doping levels of the different regions of the structure. Setting the doping level for a region typically involves four statements which include the doping distribution, region specification, dopant type, and region number. The doping distribution specifies how the doping level is spread across the region. The most commonly used and simplest distribution, called a uniform doping distribution, creates a uniform doping level across the entire region. More complex doping distributions can be used to simulate the gradual change of doping levels at the junctions of different materials with different doping levels. The region specification applies all of the statements in the doping declaration to the specified region which was numbered in the region statements. The following doping specification specifies whether the region will be *n* doped or *p* doped. An *n* doped region has excess electrons while a *p* doped

region has excess holes. The last statement specifies the concentration or dopant level. This allows the user to control the level of doping in the region. This is useful in solar cell simulations where a gradient of more highly doped materials near the contacts improves efficiency. The doping statements of a simple GaAs solar cell along with the visual representation of the doping levels are given in Figure 21. In the visual representation, which is viewed in Tonyplot, red represents higher doping levels while purple represents lower doping levels.

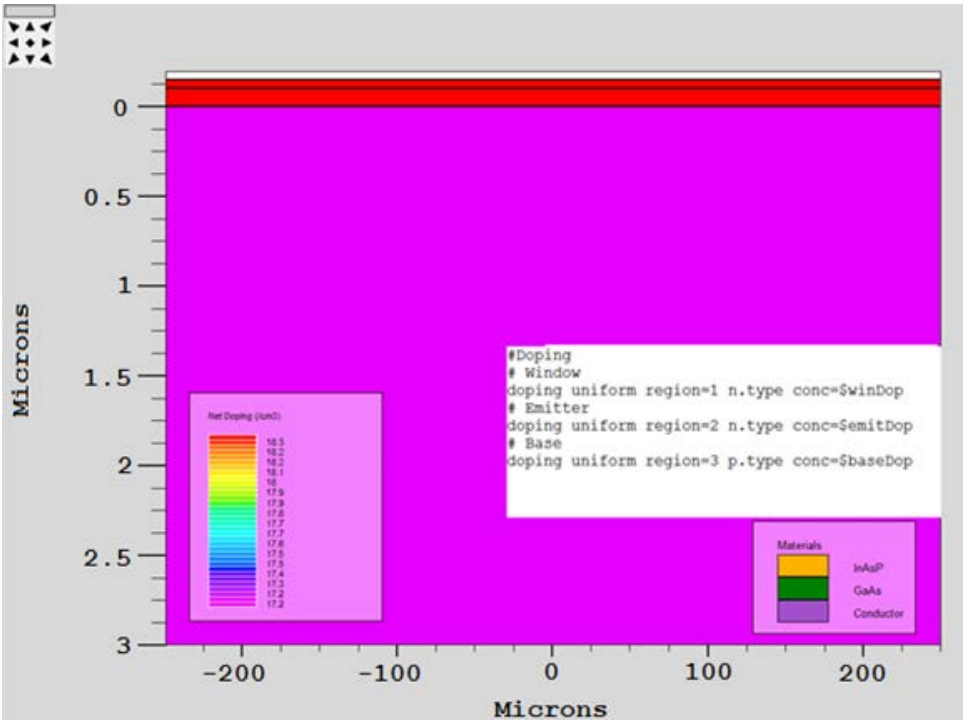

Figure 21. The Doping profile of a simple GaAs solar cell with corresponding Deckbuild input code is shown

6. Material Statements

The material defining statements that follow the definition of the device structure allow the user to alter the properties of given materials or to input new materials into the device. The statements alter the material properties of a specified metal, semiconductor, or insulator to more accurately simulate a device that uses materials which do not match the given default values of the ATLAS software. As an example, inputting the statement

material material=GaAs sopra=Gaas.nk

into Deckbuild sets the optical properties of all GaAs in the device to match the values in the "Gaas.nk" file from the sopra database of Silvaco. This statement is particularly important in modeling solar cells because the default values for the optical properties of materials do not suffice for proper solar cell simulations. The sopra database in the ATLAS software is a database that contains the optical properties of many commonly used materials. If a material is not in the sopra database, the user can create an input file to set the optical properties of that material.

The most important capability that material statements allow is the creation of user defined materials. The user can arbitrarily use any material when defining a device structure and then alter all of its pertinent properties to match that of a desired material. Though the material will carry the name of the arbitrarily picked material, it will functionally act as whatever material the user desires. This capability is pertinent in the modeling of carbon nanotube networks in this thesis.

B. OBTAINING DEVICE SOLUTIONS AND OUTPUTS

Once an input structure is defined, the user can obtain solutions to numerous conditions that the ATLAS software has the capability to simulate. In simulating solar cells, the user must specify a beam of light which shines upon the device and can then use any number of electrode conditions and solve statements to gather the desired characteristics.

1. Defining the Light Source

To evaluate a solar cell created in Deckbuild or another structure defining program, the user can simulate the actual conditions in which a solar cell would operate. This includes variables such as a light beam with an associated optical intensity and angle of incidence, different voltage conditions on the electrodes, and temperatures. In this thesis, the light beam and the electrodes are utilized to set the environment for obtaining solutions of solar cell simulations.

In Deckbuild, the light beam statement, which is used in obtaining solar cell solutions, comes after all of the structure defining statements and before the following solve statements. The light beam defining statements in this thesis include a power file, a

range of wavelengths to be sampled from the power file, and the number of samples to be taken over the range. The power file consists of wavelengths and associated power levels. This file is sampled so that the ATLAS software can obtain solutions for each wavelength's associated power level. Higher sampling values can give more accurate results but can take much longer to simulate. The statements

Beam num=1 am0 wavel.start=0.21 wavel.end=4 wavel.num=50

define a lightbeam that conforms to the default *am0* spectrum and is sampled 50 times over the wavelengths of 0.21 µm to 4 µm. The user can create and import light source data or use the default power files in the ATLAS software. The default *am0* spectrum obtained from the 2000 ASTM Standard Extraterrestrial Spectrum Reference E-490-00 which is shown in Figure 22 is utilized in this thesis.

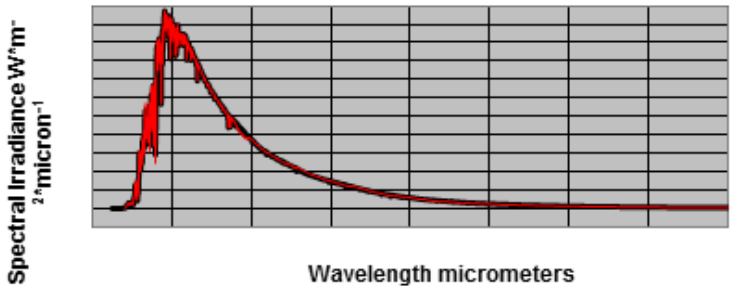

Figure 22. Spectral irradiance is graphed against wavelength of light for the standard *am0* spectrum. These values are the default value for the *am0* spectrum in Silvaco ATLAS. From [11]

2. Obtaining Solutions

Before inputting statements which obtain all of the pertinent solutions for a device, files must be created to store all of the following solutions. These files can be of two types: log and structure files. A log file must be created before any solve statement or any following calculations are not stored. The statement

log outfile=GaAs_Thermal_cell.log

creates a file named "GaAs_Thermal_cell.log" that stores all of the following solutions unless a separate log file is later defined before a different type of calculation. This file

can be viewed graphically in Tonyplot, which allows the user to specify the specific parts of the solution to graph, as many solutions are all contained in one file and cannot be graphed simultaneously.

Structure files can be saved after a specific solve statement. This file stores all of the data from the solution and allows it to be viewed visually on the device structure. An example of the resulting structure file following a solve statement is given in Figure 23. The numerical data saved into the structure file can be converted into a visual representation within the device by Tonyplot. Photogeneration rates in the solar cell were stored into the structure file in shown in Figure 23. Red and orange regions represent higher photogeneration rates while purple regions show no photogeneration.

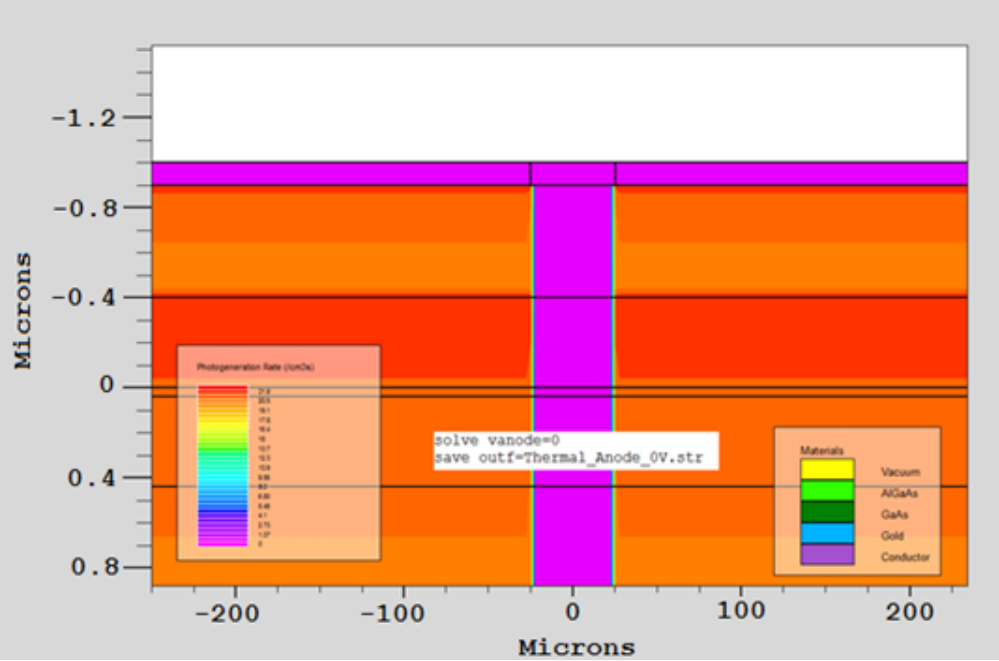

Figure 23. Photogeneration data is displayed in different areas of the solar cell with different colors specifying different photogeneration rates. Red represents higher photogeneration rates while purple represents no photogeneration

After defining a log file in which all solutions are to be stored, ATLAS software does an initial solving of the doping profile and the potential at every mesh point in the zero electrode bias case. This initial solution is obtained when there is no initial reference

zero bias solution but can be specified by the statement *solve init*. After this initial solve statement, the conditions for the specific solve statements can be set. In simulating the operation of a solar cell, the statement

solve B1=1.0

applies the equivalent of one sun from the earlier defined light source and solves the pertinent quantities such as photogeneration rates and optical intensities at each mesh point as well as the electrode currents. After the beam of light has been applied, solutions at different electrode voltages can be obtained to create the solar cell's I-V curve. The statements

solve vanode=0 name=anode vstep=0.1 vfinal=0.7

obtain solutions for the illuminated solar cell at a range of anode voltages. This statement declares an initial anode voltage of 0 V and obtains solutions in the range of 0 V to 0.7 V in increments of 0.1 V. By sweeping across anode voltages from 0 V to V_{oc} for the solar cell, the I-V curve is obtained. An I-V curve obtained by simulating a GaAs solar cell in ATLAS and sweeping anode voltages is shown in Figure 24. The simulated cell, like real solar cells, shows a characteristic in which a gradually increasing anode voltage causes lower net cathode current until the V_{oc} condition.

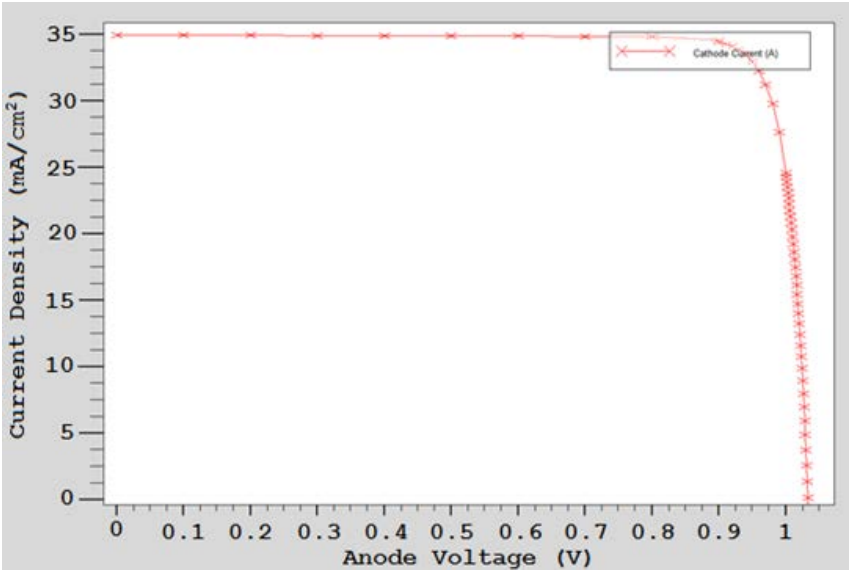

Figure 24. Anode Voltage is plotted against cathode current for an ATLAS simulated GaAs solar cell

C. CHAPTER SUMMARY

How solar cells are simulated in ATLAS software was covered in this chapter. The cell structure is defined using Deckbuild code, setting the structure mesh, regions, electrodes, doping levels, and material properties. The conditions for which solutions are to be obtained can then be set. The ATLAS software then obtains solutions for all solve statements and saves the results in log files and structure files based on the instructions of the user.

The method of modeling a CNT layer and including the model in a simulated solar cell are described in the following chapter.

V. MODELLING A HETEROGENEOUS CARBON NANOTUBE LAYER

The method used in modeling a heterogeneous layer of CNTs as a transparent charge collector in Silvaco ATLAS software is covered in this chapter. Due to the restrictions associated with modeling materials in ATLAS software, simplifications and assumptions were made to best simulate a metal-like material with certain conductance and optical properties. The assumptions made in modeling the CNT layer as well as some of the experimental data used as the basis for the model are covered in this chapter.

A. BASIS FOR THE CNT MODEL

The model for heterogeneous CNT networks created in this thesis is based on the experiments of the Institute for Microstructural Science of the National Research Council of Canada[1]. In these experiments, networks of SWCNTs were deposited onto polyethylene terephthalate (PET) films by a dip method, and the characteristics of the CNT networks were measured. This dip method utilized a solution in which a set density of SWCNTs was present. The PET films were dipped into the solution for ten seconds and withdrawn at a speed of 0.5 cm/min. The PET film was then baked in a Fisher isotherm oven at a temperature of 110 Celsius for five minutes. The data of two heterogeneous networks that were the result of one and two-dip coatings, respectively, are utilized in this thesis. These CNT networks were tested to obtain their value of sheet resistance and their level of light transmission. The light transmission of the single and double-dip coated CNT networks is shown in Figure 25. The single-dip coated CNT network has a higher value of sheet resistance of 128 ohms per square but higher net light transmission.

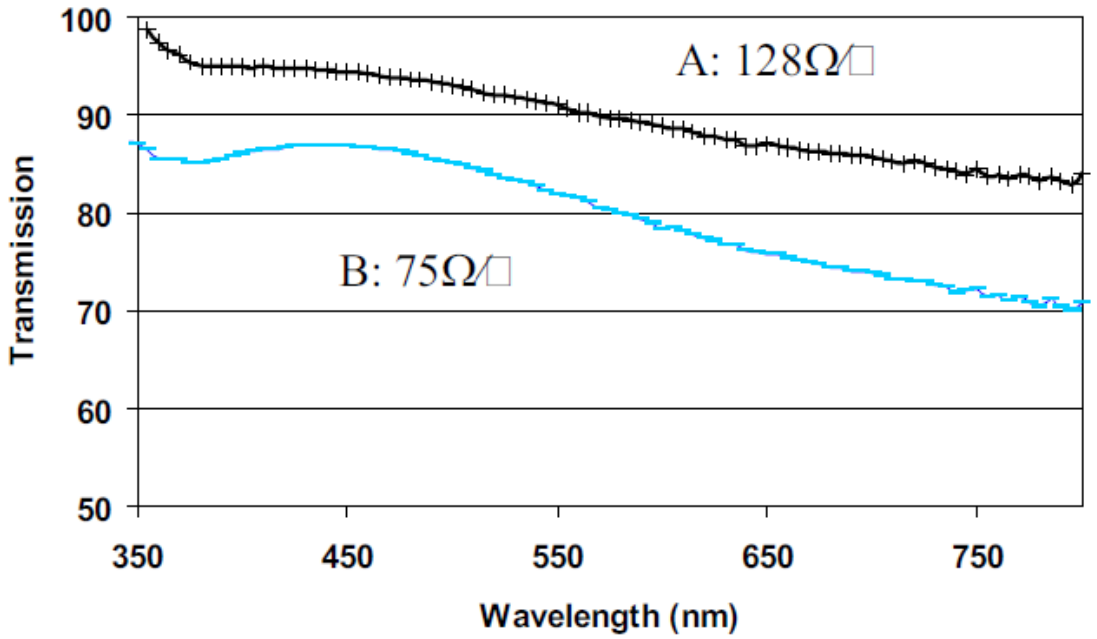

Figure 25. The experimental light transmission data of a single-dip coated and double-dip coated CNT network show an inverse relationship between sheet resistance and light transmission. From [1]

B. MODELING A TRANSPARENT CONDUCTOR IN SILVACO ATLAS

Ideally, a heterogeneous CNT network would be modeled as a metal with the optical properties and resistivity of the CNT network. However, due to the limitations of ATLAS software, the CNT network in this thesis is modeled as a low bandgap semiconductor. The ATLAS software has problems obtaining solutions when a metal makes contact with an electrode in the specified structure. Since the purpose of this thesis is to analyze the flow of charge carriers through a semitransparent material, the use of a semiconductor is optimal because the ATLAS software obtains solutions for all of the charge carriers moving towards the electrodes in semiconductors.

Though a heterogeneous CNT network does not exhibit semiconductor properties, the material statements in the ATLAS code can be utilized to create a semiconductor with metallic properties. In this thesis, 4-H Silicon Carbide (4H-SiC) was chosen as the semiconductor to alter based on the work of Brunton in the modeling of carbon nanofiber interconnects in Silvaco Atlas software[12]. To create an accurate model of a CNT

network, the material properties of Silicon Carbide were modified to give the material metallic characteristics while also matching experimental sheet resistance values. Since altering the optical properties adds unnecessary complications to the material model, the Silicon Carbide was made to be completely transparent. The input light beam was modified to instead model the resulting light that would pass through a CNT network based on experimental light transmission data.

1. Material Properties of the CNT Network Model

The heterogeneous CNT network modeled in this thesis used 4H-SiC as the base material which has the advantage of being a less commonly used material in ATLAS software. Because 4H-SiC is less commonly used than other materials in the ATLAS material library, it has fewer default parameters unimportant to this thesis that could cause errors in the simulations. The primary parameters which were modified to give the 4H-SiC metallic properties were the band and recombination parameters. The parameters that were changed in the 4H-SiC are summarized in Table 2.

The band parameters were changed to make the 4H-SiC a material with essentially no band gap and adjustable hole and electron mobilities to achieve the desired value of sheet resistance. To give the CNT network material a set value of sheet resistance, the electron and hole mobilities were modified to change the resistivity of the material. The resistivity of a semiconductor material is given by

$$\rho = \frac{1}{q(\mu_n n + \mu_p p)} \tag{6}$$

where q is the equivalent charge of one electron or hole, μ_n and μ_p are the electron and hole mobilities, respectively, and n and p are the electron and hole concentrations in the material. The sheet resistance of a material is given by

$$R_s = \frac{\rho}{t} \tag{7}$$

where t is the thickness of the material. The equation for sheet resistance was first used to solve for the necessary resistivity based upon a thickness of one micron and a sheet resistance value obtained from experimental data. The electron and hole mobilities were

then set equal to each other and solved for in the resistivity equation. Though the electron and hole mobilities are not equal in a heterogeneous CNT network, the basic creation of a sheet resistance based upon equal mobilities was adequate for the purposes of this thesis. The CNT network created in this thesis was an intrinsic, one micron thick layer of 4H-SiC. To achieve the desired values of sheet resistance, the values of *n* and *p* were set at 10^{17} cm^{-3}, the typical intrinsic carrier concentration of 4H-SiC at room temperature. The electron and hole mobilities for each value of sheet resistance were calculated to match the experimental sheet resistances of 75 Ω and 128 Ω and are given in Table 2. In Silvaco ATLAS, electron and hole mobility are abbreviated as MUN and MUP respectively.

To verify the calculations of sheet resistance, each of the modeled CNT materials was simulated with 1 V applied across the width of material as shown in Figure 26. The current was calculated in each case, and the result was used to determine the sheet resistance of each material. The two values of sheet resistance obtained were 126 Ω and 76 Ω of sheet resistance, which closely match the experimental data which the models are based on. The final parameters used in the two CNT materials are summarized in Table 2.

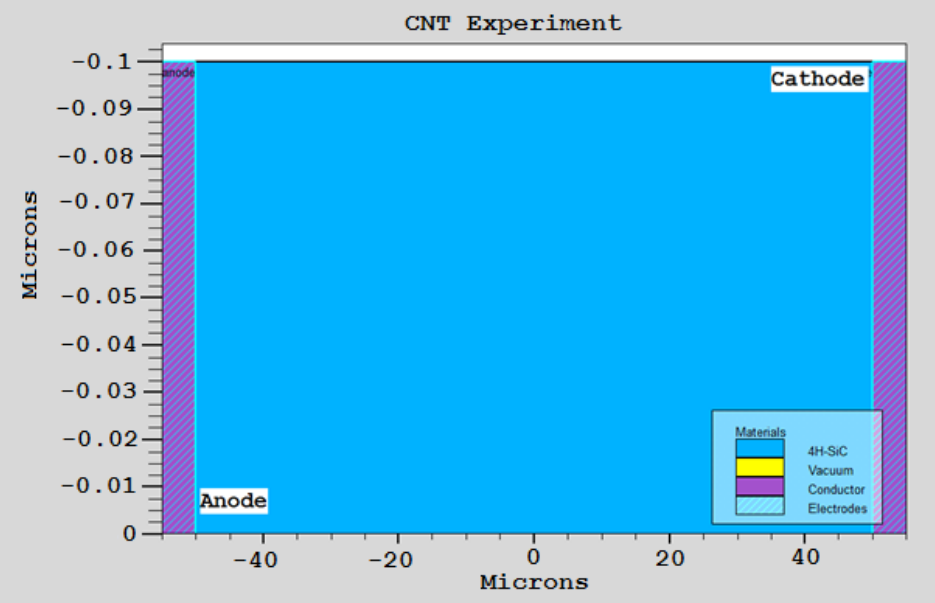

Figure 26. The experiment to determine the sheet resistance of the CNT materials is shown

Table 2. The material parameters that were changed to give 4H-SiC metallic properties in Silvaco ATLAS are summarized

Parameter Type	ATLAS Identifier	Value
Band	Permittivity	5.4
	Affinity	5.8
	NC300,NV300	$3x10^{17}$
	NC.F,NV.F	$3x10^{17}$
	MUN,MUP (126Ω)	8138.02
	MUN,MUP (76Ω)	13889
Recombination	taun0,taup0	0
	nsrhn,nsrhp	0
	ksrhcn,ksrhcp	0
	ksrhtn,ksrhtp	0
	ksrhgn,ksrhgp	0
	augn,augp	0
	augkn,augkp	0
	kaugcn,kaugcp	0
	kaugdn,kaugdp	0
	Etrap	0
	Copt	0

The other material property which significantly affected the functionality of the CNT network material was the electron affinity. The electron affinity of a material is the difference between the vacuum energy level and the conduction band energy level of a material. This property affected the CNT network material by altering the junction with the neighboring Aluminum Gallium Arsenide (AlGaAs) layer in the solar cell used in this thesis. Ideally, the CNT network acts as a metal and has a metal-semiconductor junction characteristic. However, since the CNT network in this thesis was modeled as a semiconductor, a heterojunction was created between the CNT material and the neighboring AlGaAs layer. To accurately model a heterogeneous network, the electron affinity of the material was modified until the functionality of the heterojunction with the AlGaAs layer most closely resembled the junction of a metal and a semiconductor. Ideally, this junction would not impede the flow of current, allowing for all generated charge carriers in a solar cell to reach the top contact. To determine the optimal value of

electron affinity, a GaAs solar cell with a top CNT layer was simulated with varying CNT electron affinity levels. The short circuit currents from these simulations were compared, and the maximum value was extracted. The electron affinity level of 5.8 eV, which allowed for the maximum short circuit current, was then set as the electron affinity level of the CNT material. The top portion of the cell used in the electron affinity comparison is shown in Figure 27. The cell has a top CNT layer with a neighboring AlGaAs layer. This same cell was also used in the final experiment of this thesis.

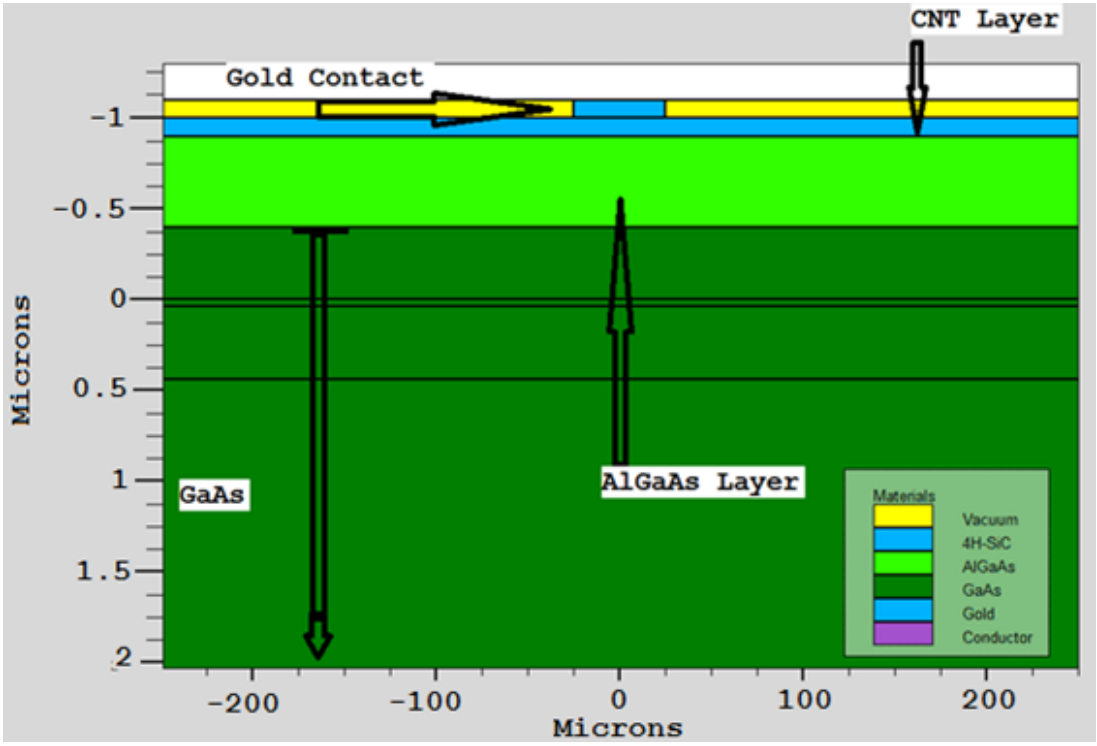

Figure 27. The top portion of the solar cell used in the electron affinity comparison is shown

2. Modeling the Optical Properties

To model the optical properties of a heterogeneous CNT network, the input solar power in simulations involving a CNT network was altered to model the resultant light transmitting through the material while leaving the CNT material completely transparent. To achieve this, the transmission data from the Institute for Microstructural Science of the National Research Council of Canada was used to apply a series of scale factors to alter the *am0* spectrum at different wavelengths[1]. The *am0* spectrum compared with the

input spectrums of associated with heterogeneous CNT layers of 76 Ω and 126 Ω of sheet resistance are shown in Figures 28 and 29. The net drop in input power with the addition of a CNT layer is shown in Figure 28. The percentage of input power present for a range of wavelengths in each of the CNT light spectrums relative to *am0* is shown in Figure 29.

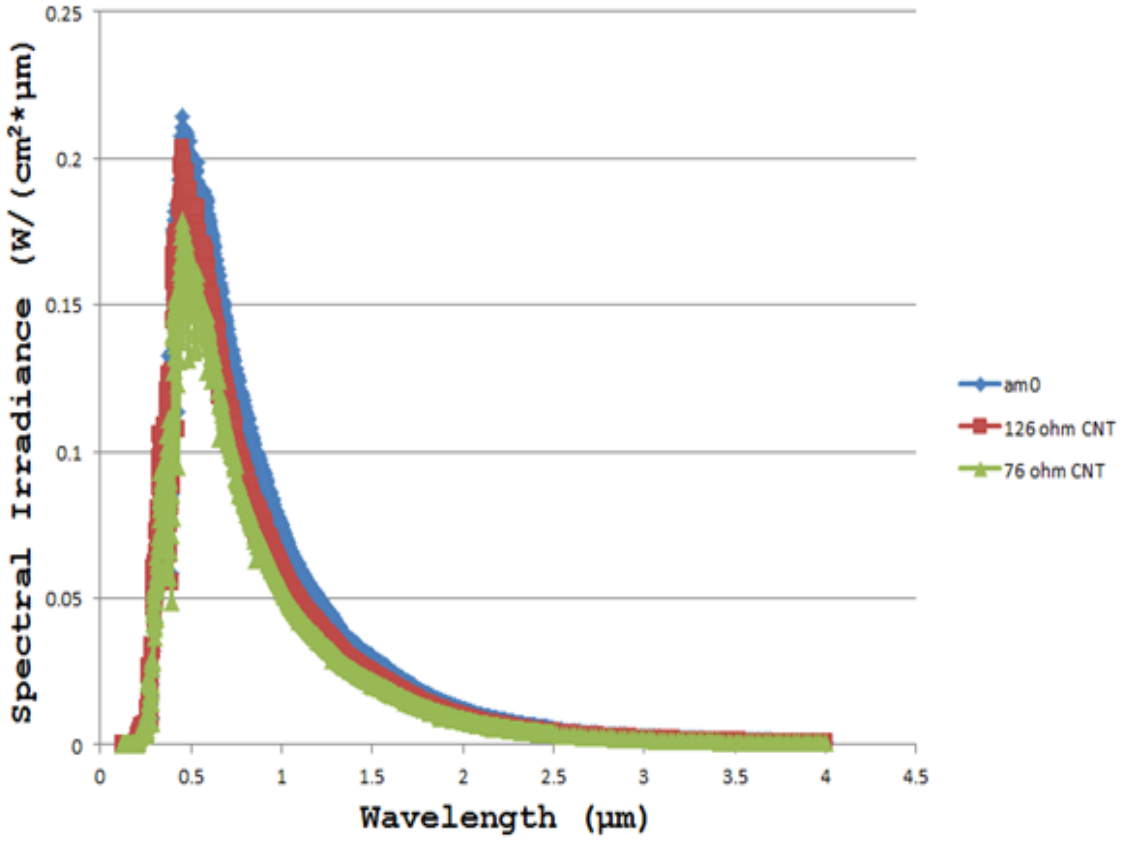

Figure 28. The *am0* spectrum is plotted against the spectrums used in simulation of CNT networks with 126 Ω and 76 Ω of sheet resistance

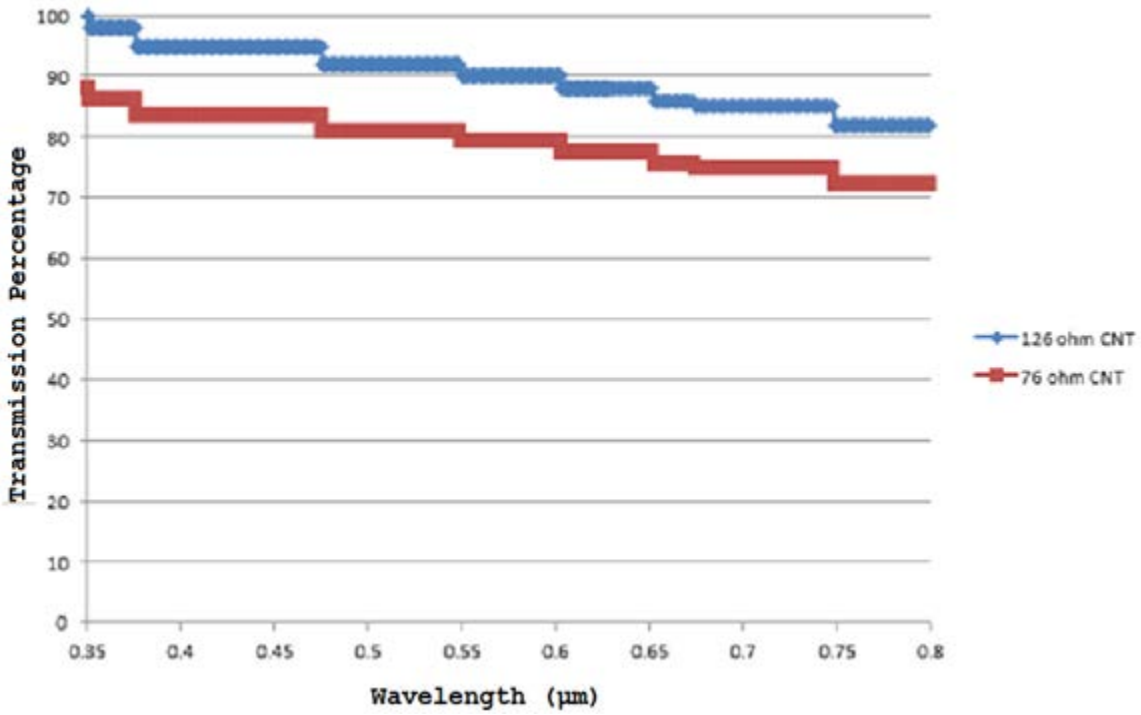

Figure 29. The power level of a range of wavelengths relative to *am0* is plotted for the input light of solar cell simulations involving CNT networks of 126 Ω and 76 Ω of sheet resistance

C. EVALUATING THE CNT MODEL IN A SOLAR CELL

In evaluating the CNT model, the most important factors to analyze were the benefits of having a lower resistance path for charge carriers to travel to the top contact of a solar cell. Therefore, experiments were set up which compared the performance of a solar cell with and without a CNT layer while varying certain aspects of the solar cell. The first experiment compared the current density in different regions of a GaAs solar cell with and without a CNT layer. This experiment demonstrated that photogenerated charge carriers were travelling through the CNT layer to the top contact.

To evaluate the performance of a CNT layer in a solar cell, an experiment was set up so that the solar cell width was varied while keeping the contact width constant in a GaAs solar cell with and without a CNT layer. The contact width was kept constant at all solar cell widths to analyze the effects of gradually increasing charge carrier distance to

the contact of the solar cell. A visual demonstration of the experiment is given in Figure 30. The width of the cell *W* was varied while solar cell parameters were obtained for each width.

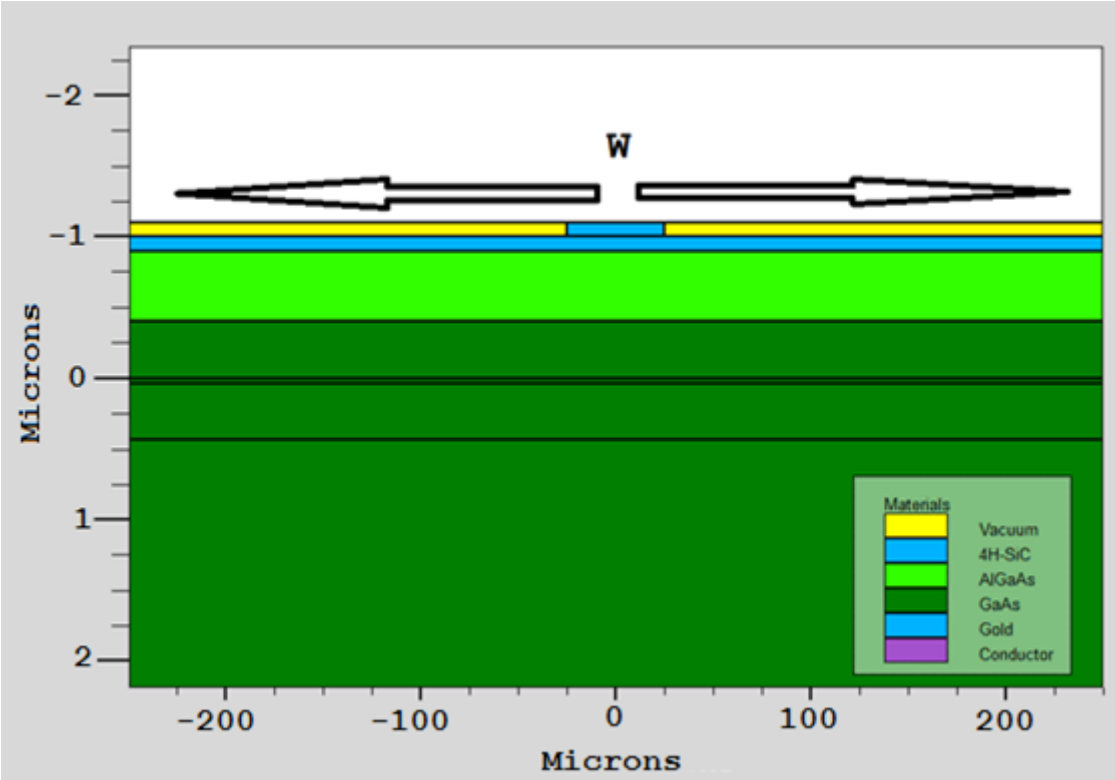

Figure 30. A visual demonstration of the experiment used to evaluate the performance of the CNT layer is shown. The cell displayed has a width of 500 microns, representing one run of the experiment

The pertinent solar cell characteristics gathered in each cell width simulation were I_{sc}, V_{oc}, P_{max}, V_{max}, and I_{max}. These parameters were obtained at each width for a GaAs solar cell without a CNT layer, the GaAs solar cell with a CNT layer of 126 Ω of sheet resistance, and the GaAs solar cell with a CNT layer of 76 Ω of sheet resistance. The parameters were then compared to evaluate the effect of a CNT layer on a GaAs solar cell.

D. CHAPTER SUMMARY

The method of modeling a heterogeneous CNT layer for solar cell applications in Silvaco ATLAS software was covered in this chapter. The CNT layer was given specific sheet resistance values by altering the electron and hole mobilities for a constant layer thickness of one micron. The optical properties of the material were accounted for by altering the input solar spectrum to the simulated solar cell while keeping the CNT layer completely transparent. The *am0* spectrum was altered so that it matched the resulting input light power that would transmit through a CNT layer of given sheet resistance based on experimental spectral data from the Institute for Microstructural Science of the National Research Council of Canada.

The experiments which were used to evaluate the effects of a CNT layer on the surface of a solar cell were then described. The current densities of solar cells with and without top CNT layers were first compared to verify that photogenerated carriers were travelling to the top contact via the CNT material. A GaAs solar cell with and without a CNT layer was then simulated with varying solar cell width and a constant contact width. The pertinent cell parameters were then compared to analyze the effects of a lower resistance path for charge carriers in the GaAs solar cell. The results of these experiments are given in the next chapter.

VI. RESULTS

The experiments described in the previous chapter were conducted on GaAs solar cells with and without a top CNT layer. The results were obtained and analyzed to determine the functionality of the modeled top CNT layer on a solar cell.

A. VERIFICATION OF THE CNT LAYER AS A CHARGE COLLECTOR

A GaAs solar cell was first simulated with and without a CNT layer, and the current densities in different regions of the cells were analyzed to verify that charge carriers were travelling in the CNT layer to the top contact. The GaAs solar cell used in this thesis is based on the work of Crespin[13]. The cells were simulated in the short circuit condition in which no bias was applied across the electrodes. The gold top contact was set to be opaque to cause shadowing as in real solar cells. This effect blocks light to a portion of the cell, preventing photogeneration in the shaded region. The resultant photogeneration rates for a 500 micron wide GaAs cell with a 50 micron wide gold contact are shown in Figure 31. The gold contact blocks light to ten percent of the cell, essentially preventing the generation of charge carriers.

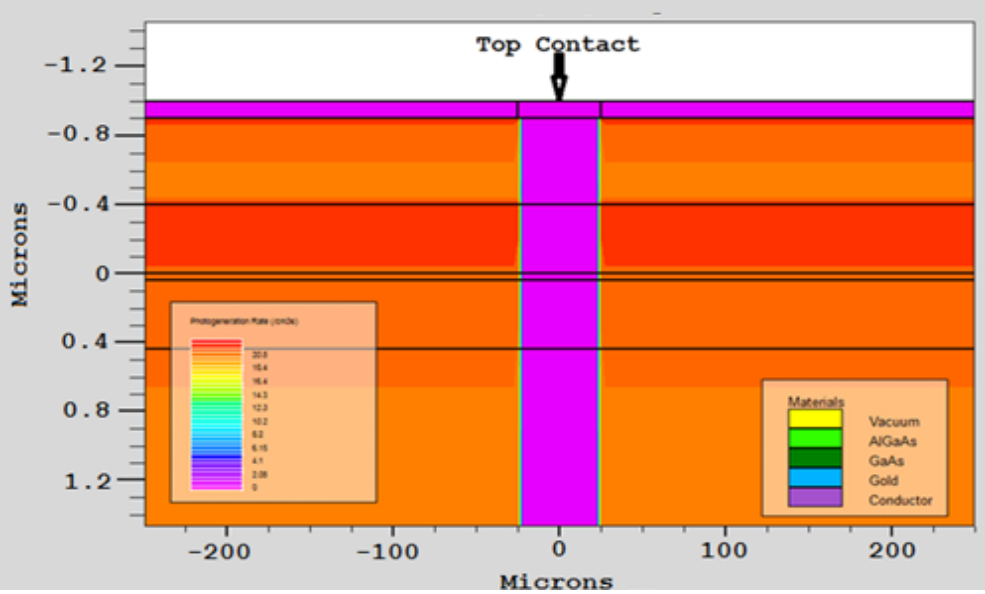

Figure 31. Photogeneration in a GaAs cell with a gold top contact is shown. Red and orange regions have higher photogeneration rates while purple regions exhibit no photogeneration

The total current density in a GaAs solar cell without a CNT Layer is shown in Figure 32. The current concentrates in the top AlGaAs layer and the GaAs emitter region when travelling to the top contact. The flow of charge carriers in this region causes a voltage drop as the charge carriers are affected by the resistance in both of these regions.

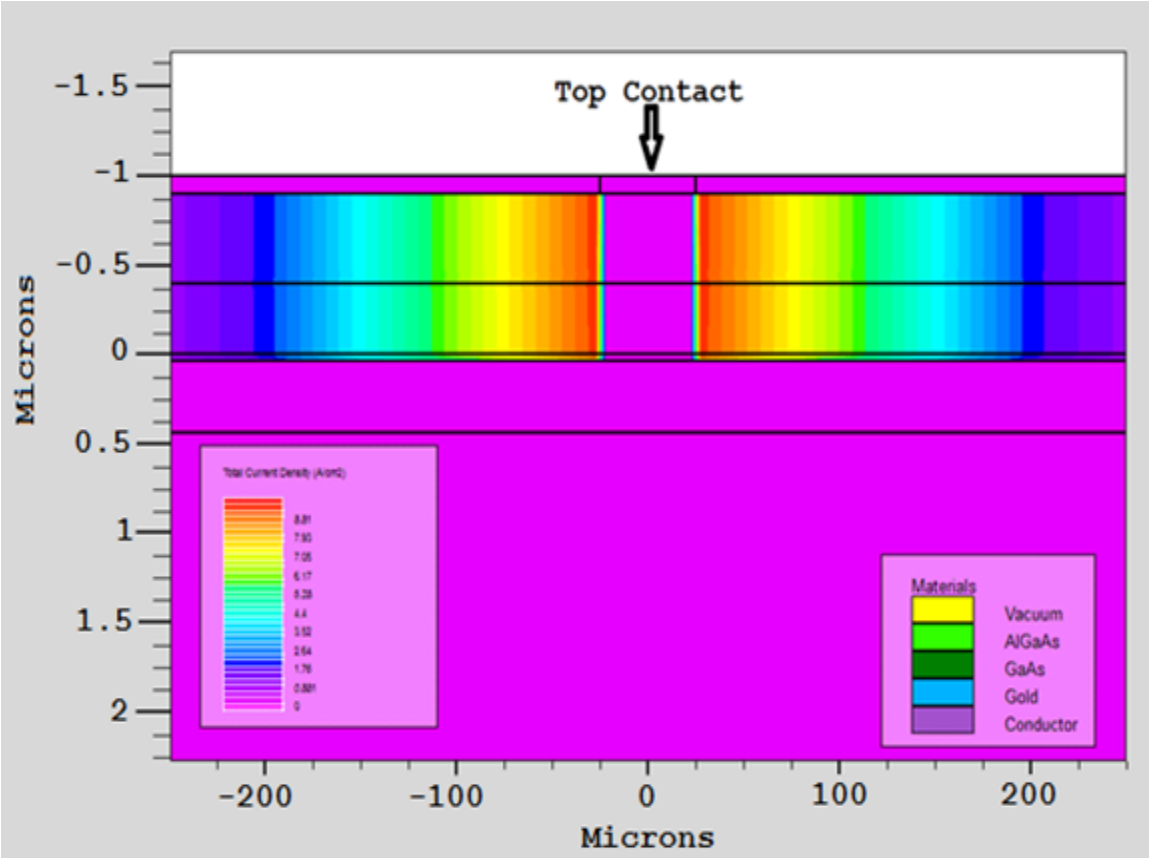

Figure 32. Current Density viewed in Tonyplot for a GaAs solar cell is shown

The current density in a GaAs solar cell with a top CNT layer of 126 Ω of sheet resistance is shown in Figure 33. The current converges in the top CNT layer to travel to the top contact for charge collection. The charge carriers in this region see less net resistance in the more highly conducting CNT layer.

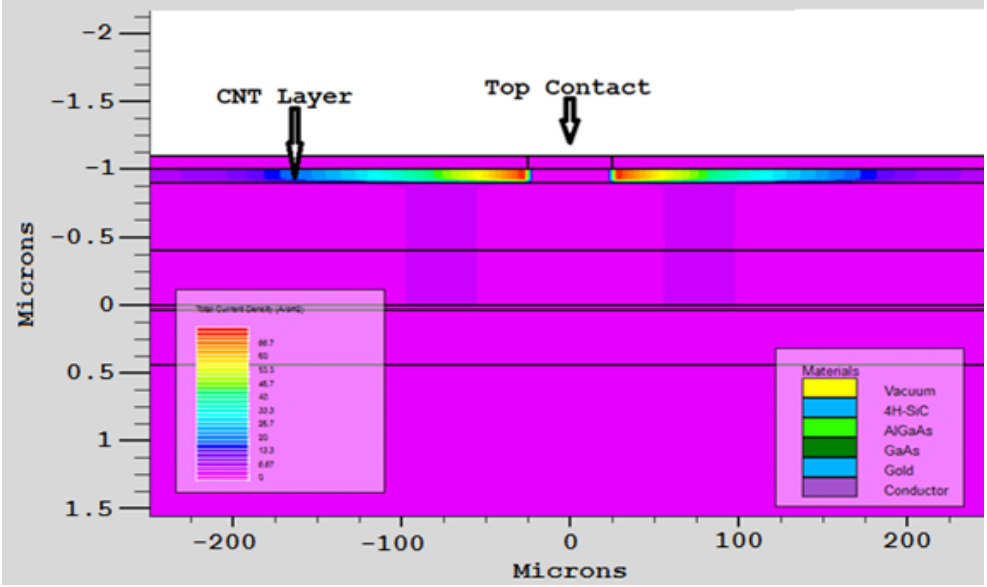

Figure 33. The current density in a GaAs solar cell with a 126 Ω sheet resistance layer of CNT on the surface is shown

The current density in the GaAs solar cell with a 76 Ω sheet resistance CNT layer on the surface is shown in Figure 34. Like the 126 Ω CNT layer cell, the current converges in the top CNT layer as charge carriers travel along the path of least resistance.

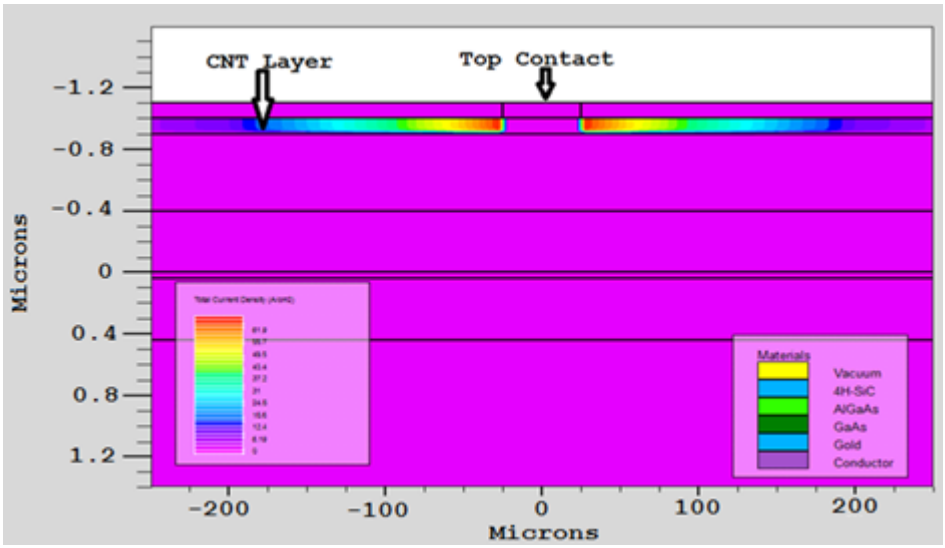

Figure 34. The current density in a GaAs solar cell with a 76 Ω sheet resistance layer of CNT on the surface is shown

Once the current was shown to travel through the top CNT layer, the I-V characteristic for the GaAs solar cell was compared with the I-V characteristic of the GaAs cell including top CNT layers of 126 Ω and 76 Ω of sheet resistance. These solar cells were all simulated with the inputs outlined in the previous chapter which are based on the amount of *am0* input light present to the solar cell after transmission through a CNT layer. The cell width was set at 500 microns in these simulations. The ATLAS code used to simulate the cells is given in the Appendix. The I-V curves for the normal GaAs solar cell, a cell including a 126 Ω sheet resistance CNT layer and a cell including a 76 Ω sheet resistance CNT layer are shown in Figure 35. As expected with a smaller cell width, the cells with the CNT layers have lower current values than the standard GaAs cell due to the loss of input power caused by the CNT layers. A comparison of solar cell parameters is given in Table 3.

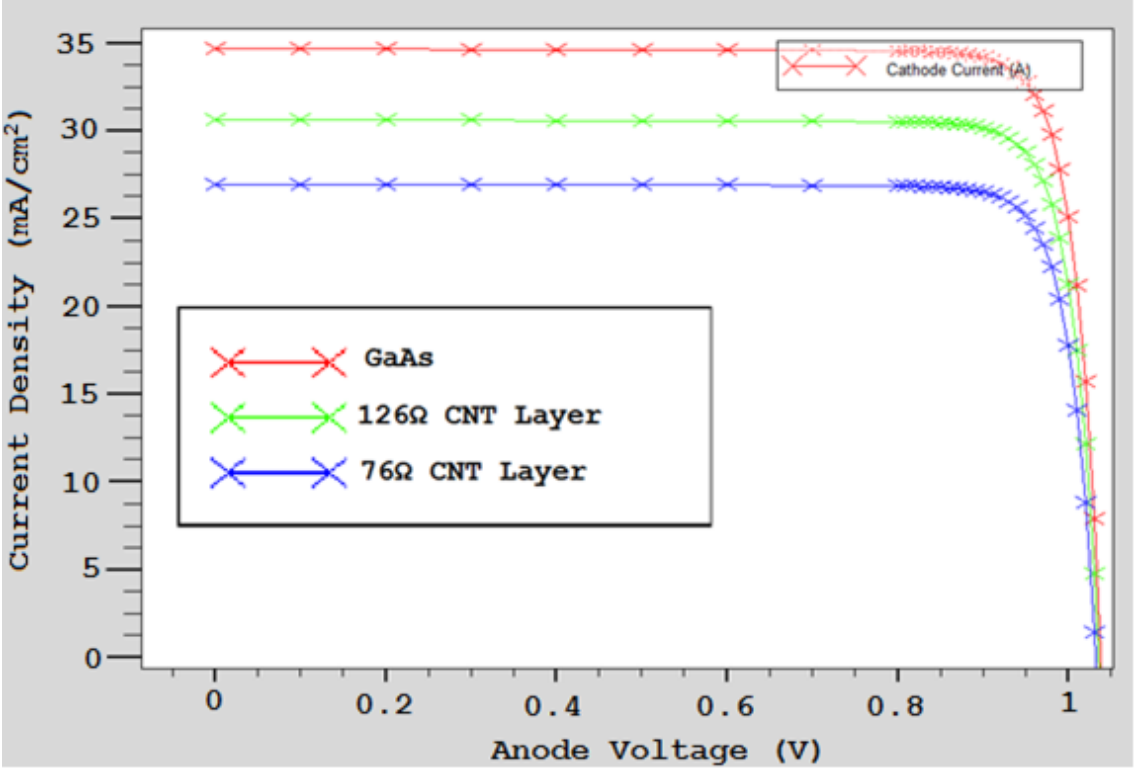

Figure 35. The I-V curves for the standard GaAs solar cell and GaAs solar cells including top CNT layers of 126 Ω and 76 Ω of sheet resistance are shown

Table 3. A summary of the important solar cell parameters is given for the standard 500 micron wide GaAs solar cell and the cell with different CNT layers

Cell Type	GaAs	126 Ω CNT	76 Ω CNT
Cell Width (μm)	500	500	500
I_{sc} (mA/cm^2)	34.691	30.637	26.96
V_{oc} (V)	1.037	1.035	1.031
P_{max} (W/cm^2)	31.274	27.519	24.163
V_{max} (V)	0.94	0.93	0.93
I_{max} (mA/cm^2)	33.272	29.591	25.982

B. VARYING THE CELL WIDTH

The next experiment carried out was outlined in the previous chapter. The GaAs cell along with the two cells with CNT layers were simulated at varying widths while gathering the solar cell parameters. The contact width was held at a constant value to demonstrate the advantages of a lower resistance path for charge carriers at greater cell widths. In the experiment the cell width was varied from 200 to 4000 microns, and the contact width was set at 50 microns for all simulations. The full code used in the simulation is given in the Appendix.

The first cell parameter analyzed for each of the solar cells was the short circuit current. The short circuit currents for each cell obtained during the simulation are shown in Figure 36. For each of the cells, the short circuit current gradually increased as the cell width increased. This result is expected as gradual increases in cell width paired with a constant contact width result in a gradual decrease in the percentage of the cell being shaded by the contact. With the minimum simulated cell width of 200 microns, 25 percent of the cell cannot generate charge carriers, while with the maximum cell width of 4000 microns, just over one percent of the cell is shaded.

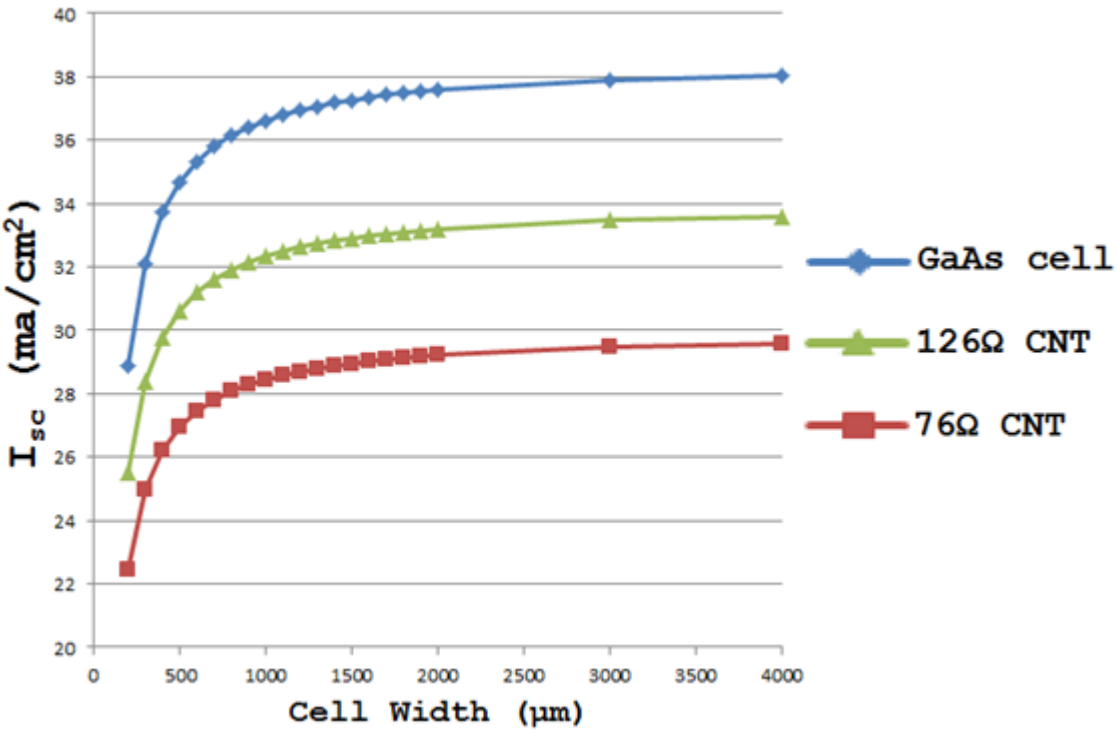

Figure 36. The short circuit current obtained at each cell width simulated is plotted for a GaAs solar cell and cells with 126 Ω and 76 Ω sheet resistance layers

The open circuit voltages of the three solar cells were then analyzed and compared. The open circuit voltages of the three cells graphed against cell width is shown in Figure 37. The slight increase in all of the open circuit voltages is caused by the reduction in shading. As less of the cell is shaded, more charge carriers are generated in the cell. The open circuit voltage is the voltage caused by the concentration of opposing charge carriers at the two electrodes of the solar cell. As more charge carriers are generated, the potential between the two electrodes connected in an open circuit configuration becomes greater.

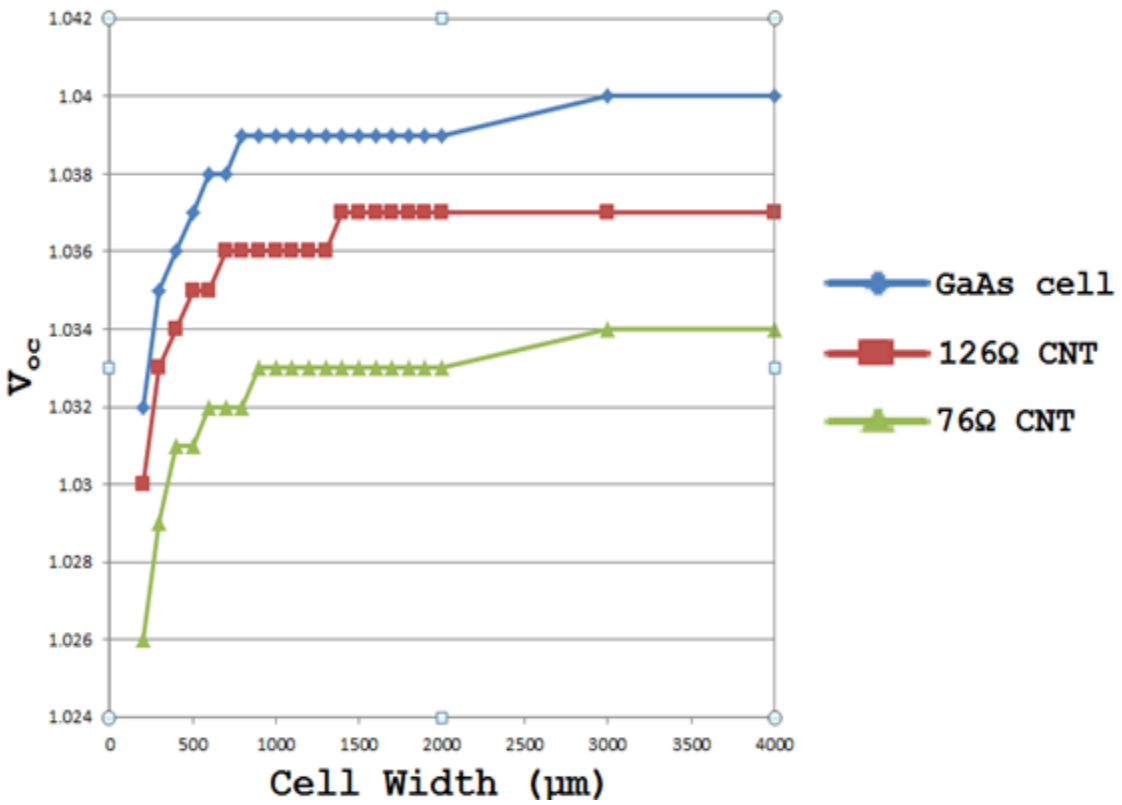

Figure 37. The open circuit voltage obtained at each cell width simulated is plotted for a GaAs solar cell and cells with 126 Ω and 76 Ω sheet resistance layers

The maximum power values for each solar cell were then obtained and compared for each cell width and are shown in Figure 28. Each cell reached a maximum P_{max} at a certain width and then showed reductions in P_{max} for greater widths. The most pronounced decline in P_{max} for greater cell widths was seen in the GaAs solar cell without a CNT layer. This sharp decline was due to the voltage losses from resistance in the AlGaAs and GaAs layers as charge carriers had to travel further to the contact. Since the CNT layers provided charge carries in the other solar cells with lower resistance paths to the contact, the reduction in P_{max} for greater cell widths was less pronounced.

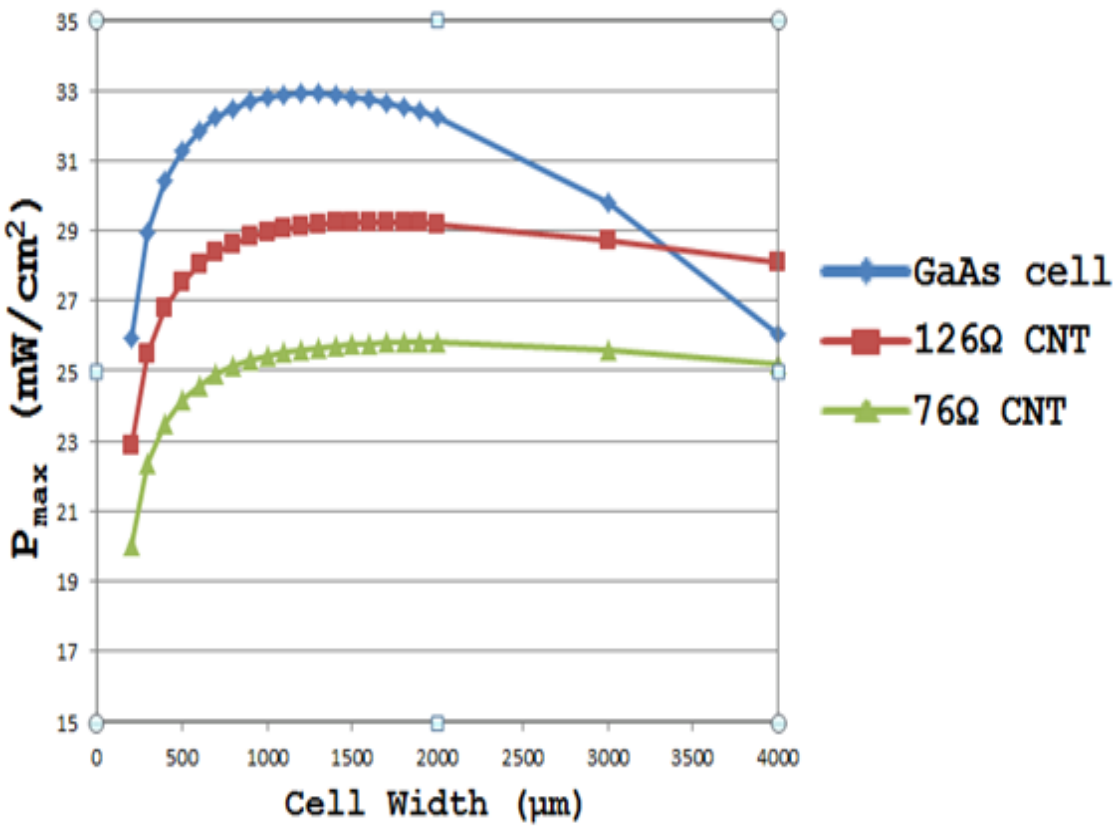

Figure 38. The maximum power obtained at each cell width simulated is plotted for a GaAs solar cell and cells with 126 Ω and 76 Ω sheet resistance layers

To verify that the voltage drop caused by charge carriers travelling to the top contact was indeed the root of reduced P_{max} for relatively large cell widths, the current and voltage at each maximum power point was obtained and analyzed. The I_{max} obtained at each cell width for the three simulated solar cells are shown in Figure 39. The GaAs cell shows a slight reduction in current at the maximum power point as the width becomes relatively large. However, this slight reduction does not account for the large drops in P_{max} seen for relatively large cell widths. The cells with CNT surface layers show a gradual increase in the current at the maximum power point regardless of cell width.

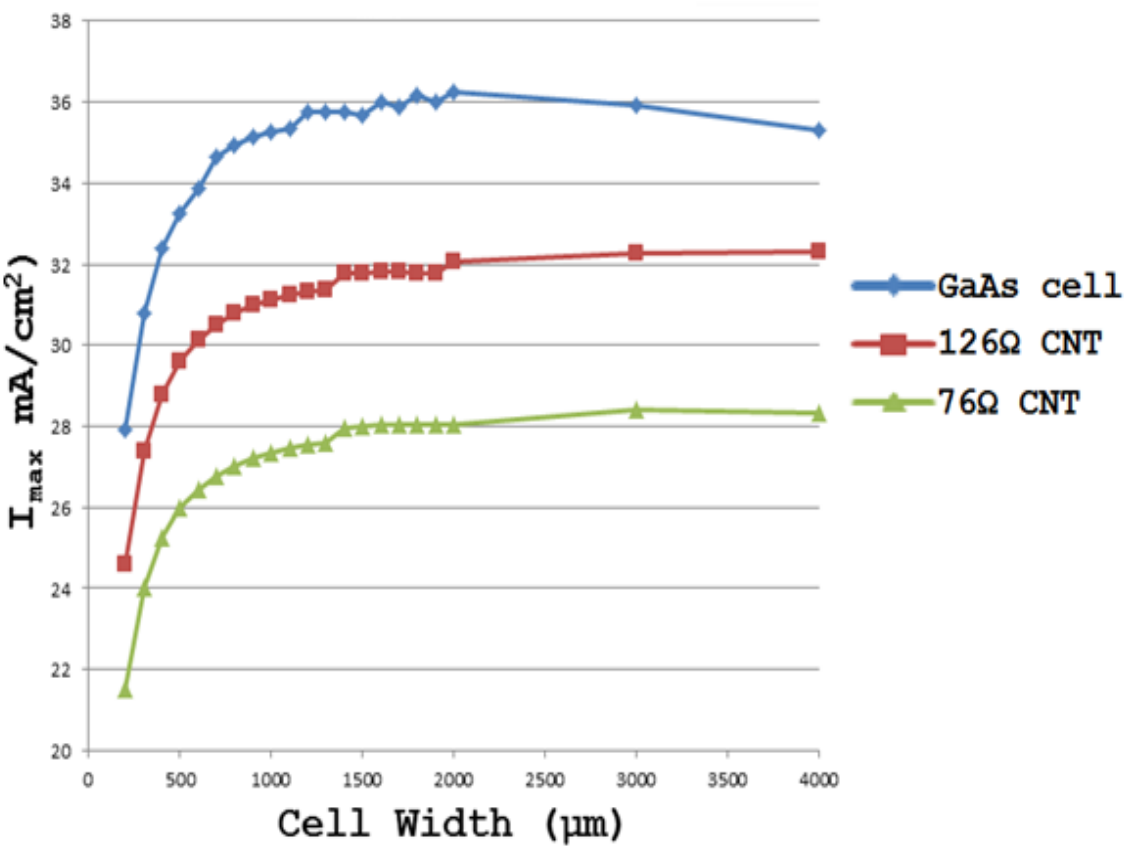

Figure 39. The current at the maximum power point obtained at each cell width simulated is plotted for a GaAs solar cell and cells with 126 Ω and 76 Ω sheet resistance layers

The voltages at the maximum power points were confirmed to be the root of the reduced P_{max} for greater cell widths and were compared to show how cell width created voltage reduction in the maximum power. The V_{max} obtained at each cell width for the three simulated solar cells are shown in Figure 40. The GaAs solar cell had the greatest degredation in V_{max} with increasing cell width. The lower sheet resistance CNT layer showed the least amount of V_{max} reduction due to the lower voltage losses from charge carriers travelling to the contact. The two cells with CNT layers on the surface clearly show an improvement in the maximum power voltage over the GaAs cell.

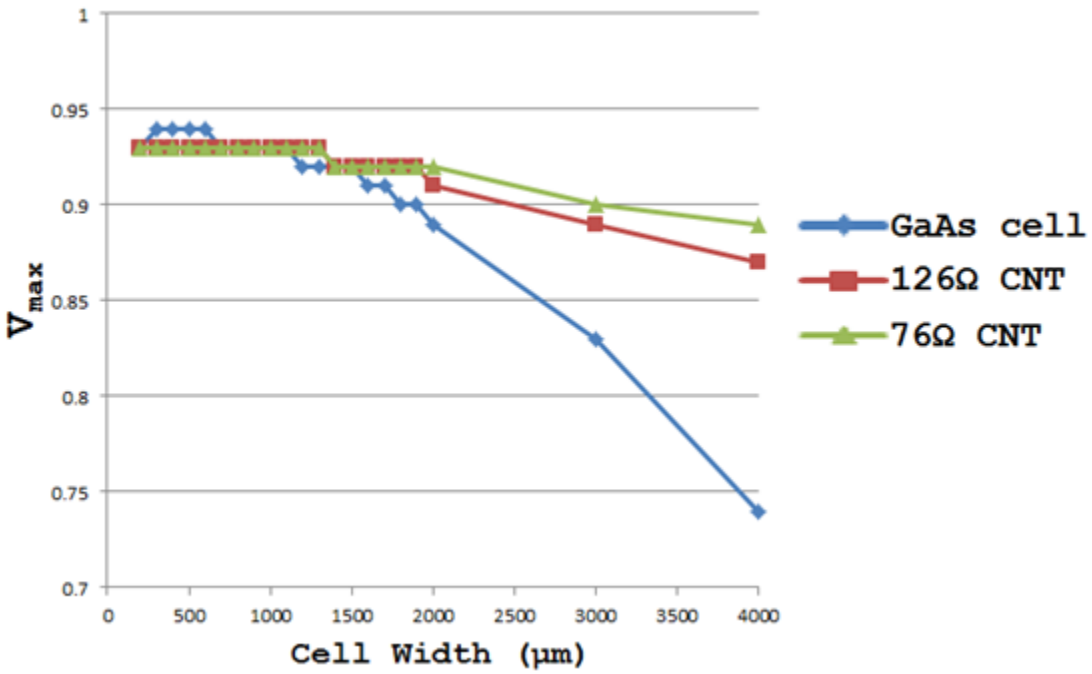

Figure 40. The voltage at the maximum power point obtained at each cell width simulated is plotted for a GaAs solar cell and cells with 126 Ω and 76 Ω sheet resistance layers

C. CHAPTER SUMMARY

The results of simulations of GaAs cells with CNT layers on the surface of the cell were presented in this chapter. The results show that the CNT model provides a lower path of resistance for charge carriers in a solar cell to travel to the top contact. The lower path of resistance was shown to improve the performance of solar cells with relatively large widths by reducing the voltage drop caused by charge carriers travelling to the top contact of a cell.

Though the solar cells with CNT layers did not show a net improvement in efficiency, the benefits of less voltage loss from charge carriers travelling to the contact can eventually improve the efficiencies of solar cells as CNT fabrication methods improve. CNT layers with lower sheet resistance and a higher level of light transmission can greatly improve the efficiency of solar cells.

VII. CONCLUSIONS AND RECOMMENDATIONS

A method of modeling heterogeneous CNT networks in Silvaco ATLAS software for photovoltaic applications was presented. This model was incorporated into a GaAs solar cell and was shown to reduce losses from the flow of charge carriers to the top contact. The unique properties of CNT layers on the surface of solar cells allow for better charge carrier collection while only losing a portion of light input power based on the light transmission of the CNT layer.

The experiments in this thesis showed that when a top CNT layer is applied to a solar cell, current congregates in the top layer and travels to the contact via a lower resistance path. As the distance charge carriers have to travel to reach the top contact of solar cell increases, the voltage drop caused by resistance in semiconductor materials was shown to have a significant effect on the maximum power available from a solar cell. The addition of a CNT layer was shown to minimize this voltage drop and maintain high maximum power levels for cells with large distances between contacts. The ability to have greater separation between top contact grid lines can allow for a reduction of the shaded area in a solar cell while also maintaining relatively wide metal top contacts in the contact grid. This is optimal since any other reduction in the shaded area without the power reductions due to semiconductor resistance in the cell requires thinner metal grid lines. The flow of current in these grid lines causes losses that increase with a decrease in grid line thickness. Since a CNT layer allows equivalent or lesser levels of net cell shading with wider top contacts, grid line losses can be reduced or made constant while reducing cell shading. This allows for greater overall efficiencies for solar cells.

Solar cells are currently a high priority for the military and the civilian sector as a viable source of renewable energy and as a power source in remote locations such as space or isolated regions. Research regarding the improvement in efficiency of solar cells will continue as nations attempt to generate more renewable energy for domestic use and new technologies require more power to be available in remote areas.

The research in this thesis provides a possible method for increasing the efficiencies of solar cells. Further research could be conducted either in improving the CNT model or by optimizing the relationship between transparency and conductivity in heterogeneous CNT networks to provide the greatest overall efficiency for a solar cell utilizing a CNT top layer. Improvements in CNT fabrication methods will also improve the possibilities for optimizing solar cell performance. The model presented in this thesis is based on specific experimental data from a fabricated CNT network. CNT networks are gradually improving in terms of transparency and conductivity. These improvements may allow solar cell efficiencies to be improved.

The model presented in this thesis is based on many simplifications to allow for a usable model in ATLAS software. Charge carrier mobility was set at a constant equivalent value for holes and electrons. Heating in the CNT layer was not accounted for and could affect the conductivity of the layer. Later research could focus on accounting for all of the physical properties of CNT layers. As more research is conducted on semi-transparent heterogeneous CNT networks, more data will be available about the physical properties of the material. These properties could be accounted for in ATLAS software, which offers a wide variety of physical models for numerous properties.

With the working model for heterogeneous CNT networks presented in this thesis, supplementary work in the optimization of solar cells is possible. The relationship between the transparency and conductivity can be used to optimize the efficiency of a solar cell. By iterating cell simulations of different widths with CNT layers of varying resistance, a maximum efficiency for different types of solar cells incorporating CNT layers could be obtained. This work could then be verified by testing on an actual solar cell to verify the model.

The ability of Silvaco ATLAS software to simulate modeled materials shown in this and other theses has important implications for the future of solar cell research. New materials can be modeled and simulated cheaply before large investments are required for physical tests. Through this modeling and simulation, solar cells can be more cheaply improved, making them a more viable power source for all applications.

APPENDIX

The following Deckbuild code was used to simulate a GaAs solar cell with and without heterogeneous CNT surface layers. The code uses loop statement to loop through different cell widths for each type of cell. The results are extracted from each run with extract statements which import the data to the "results.final" file. This file is automatically generated by ATLAS.

```
# Adam Garfrerick
# Final Experiment evaluating CNT model performance
#Definition of constants
#Mesh
#X-Mesh
#Y-Mesh
#Regions
#Electrodes
#Doping
#Material Properties
#Models
#Light Beams
#Solving

#GaAs solar cell without a CNT Layer
#The cell width is initially set at 200 microns. The loop statement is #set to loop the simulation 19 times to extract cell parameters at #varying widths

set cellWidth=200
loop steps=19
go atlas

#Constants which are used to set the cell parameters are defined

set contWidthpercent=10
set divs=10
set emitThick=0.4
set emitDepThick=.04
set baseDepThick=.4
set baseThick=10
set winThick=0.5
set contThick=0.1
set elecThick=0.1
set subThick=10
set emitMax=0
set emitDepMax=$emitMax+$emitDepThick
set baseDepMax=$emitDepMax+$baseDepThick
set baseMax=$baseDepMax+$baseThick
set baseMid=$baseMax-$baseThick/2
set subMax=$baseMax+$subThick
set winMax=$emitMax - $emitThick
set contMax=$winMax-$winThick
```

```
set contMin=$contMax-$contThick
set elecMin=$contMax-$elecThick

set winDop=1e18
set emitDop=1e18
set emitDepDop=1e18
set baseDepDop=1e17
set baseDop=1e17
set subDop=5e17

set cellWidthDiv=$cellWidth/$divs
set width3d=100e6/$cellWidth
set contWidth=25
set contWidthDiv=$contWidth/($divs)
set cellWidthHalf=$cellWidth/2

set contDiv=$contThick/($divs*10)
set winDiv=$winThick/$divs
set emitDiv=$emitThick/$divs
set emitDepDiv=$emitDepThick/$divs
set baseDepDiv=$baseDepThick/$divs
set baseDiv=$baseThick/$divs
set subDiv=$subThick/$divs

#Meshing
mesh width=$width3d
#mesh space.mult=1
#X-mesh:  Surface=500 um2 = 1/200000 cm2
x.mesh loc=-$cellWidthHalf spac=$cellWidthDiv
x.mesh loc=-$contWidth spac=$contWidthDiv
x.mesh loc=$contWidth spac=$contWidthDiv
x.mesh loc=$cellWidthHalf spac=$cellWidthDiv
#Y-Mesh
#Top of Contact
y.mesh loc=$contMin spac=$contDiv
#Window
y.mesh loc=$contMax spac=$contDiv
y.mesh loc=$winMax spac=$winDiv
# Emitter
y.mesh loc=$emitMax spac=$emitDiv
# Depletion Region
y.mesh loc=$emitDepMax spac=$emitDepDiv
y.mesh loc=$baseDepMax spac=$baseDepDiv
# Base
y.mesh loc=$baseMax  spac=$baseDiv
# Substrate
y.mesh loc=$subMax  spac=$subDiv




# Regions
# Contact
#Contact region is initially set as a vacuum region but will be covered #by a gold electrode in the electrode statements
```

```
region num=1 material=Vacuum x.min=-$contWidth x.max=$contWidth\ y.min=$contMin
y.max=$contMax
# Empty Space
region num=2 material=Vacuum x.min=-$cellWidthHalf  x.max=-$contWidth\ y.min=$contMin
y.max=$contMax
region num=3 material=Vacuum x.min=$contWidth x.max=$cellWidthHalf\ y.min=$contMin
y.max=$contMax
# Window
region num=4 material=AlGaAs x.comp=0.9 x.min=-$cellWidthHalf\ x.max=$cellWidthHalf
y.min=$contMax y.max=$winMax
# Emitter
region num=5 material=GaAs x.min=-$cellWidthHalf x.max=$cellWidthHalf\ y.min=$winMax
y.max=$emitMax
# Emitter Depletion Region
region num=6 material=GaAs x.min=-$cellWidthHalf x.max=$cellWidthHalf\ y.min=$emitMax
y.max=$emitDepMax
# Base Depletion Region
region num=7 material=GaAs x.min=-$cellWidthHalf x.max=$cellWidthHalf\ y.min=$emitDepMax
y.max=$baseDepMax
# Base
region num=8 material=GaAs x.min=-$cellWidthHalf x.max=$cellWidthHalf\ y.min=$baseDepMax
y.max=$baseMax
# Substrate
region num=9 material=GaAs x.min=-$cellWidthHalf x.max=$cellWidthHalf\ y.min=$baseMax
y.max=$subMax


#Electrodes
electrode name=anode material=Gold x.min=-$contWidth x.max=$contWidth\ y.min=$contMin
y.max=$contMax
electrode name=cathode x.min=-$cellWidthHalf x.max=$cellWidthHalf\ y.min=$subMax y.max=$subMax

#Doping

# Window
doping uniform region=4 p.type conc=$winDop
# Emitter
doping uniform region=5 p.type conc=$emitDop
#Emitter Depletion Region
doping uniform region=6 p.type conc=$emitDepDop
#BaseDepletion Region
doping uniform region=7 n.type conc=$baseDepDop
# Base
doping uniform region=8 n.type conc=$baseDop
# Substrate
doping uniform region=9 n.type conc=$subDop

#Material Properties
material TAUN=1e-7  TAUP=1e-7  COPT=1.5e-10  AUGN=8.3e-32  AUGP=1.8e-31

#Vacuum
material material=Vacuum real.index=3.3  imag.index=0

#GaAs
```

```
material material=GaAs EG300=1.42   PERMITTIVITY=13.1   AFFINITY=4.07
material material=GaAs   NC300=4.7e17  NV300=7e18
material material=GaAs   sopra=Gaas.nk

# AlGaAs
material material=AlGaAs EG300=1.5487 PERMITTIVITY=12.616 AFFINITY=3.96
material material=AlGaAs NC300=1.39e18 NV300=9.78e18 COPT=1.8e-10\ TAUN0=4.5e-9 TAUP0=2e-
8
material material=AlGaAs sopra=Algaas9.nk

# Material Properties
#CNT material properties
material material=4H-SiC  EG300=0.026  PERMITTIVITY=5.4 AFFINITY=5.8
material material=4H-SiC  NC300=3e17  NV300=3e17
material material=4H-SiC  NC.F=0  NV.F=0
# Recombination Parameters
material material=4H-SiC  taun=0  taup=0  etrap=0
material material=4H-SiC  augn=0  augp=0
material material=4H-SiC  augkn=0  augkp=0
material material=4H-SiC  kaugcn=0  kaugcp=0
material material=4H-SiC  kaugdn=0  kaugdp=0
material material=4H-SiC  copt=0
#Optical Parameters
material material=4H-SiC  real.index=1  imag.index=0

#Gold
material material=Gold real.index=1.2 imag.index=1000



#Models
models conmob consrh

output con.band val.band

#Light Beams
beam num=1  am0  wavel.start=0.21  wavel.end=4  wavel.num=50

#Output and Display Struct File


#Solving
log outfile=GaAs_Thermal_cell.log
solve init
method gummel  maxtraps=10  itlimit=25
solve B1=1.0
solve vanode=0  name=anode  vstep=0.1  vfinal=0.8
solve vanode=0.8  name=anode  vstep=0.01  vfinal=1.05

#Extract the cell characteristics for each cell width
#Results will appear in the “results.final” which is the        #default file name for extracted values in
ATLAS code

extract init infile="GaAs_Thermal_cell.log"
extract name="opt_int" max(beam."1")
```

```
extract name="Isc" y.val from curve(V."anode", I."cathode") where\ x.val=0
extract name="Voc" x.val from curve(V."anode", I."cathode") where\ y.val=0
extract name="Pm" max(curve(V."anode",(V."anode"*I."cathode")))
extract name="Vm" x.val from\ curve(V."anode",(V."anode"*I."cathode"))\ where y.val=$"Pm"
extract name="Im" $"Pm"/$"Vm"
extract name="FF" $"Pm"/($"Isc"*$"Voc")
extract name="eff" (abs($"Pm")/$opt_int)

#Code will loop again with a wider cell width. Code will loop until set #iterations complete.


set cellWidth=$cellWidth + 100

l.end

# Begin loop with 126 ohm sheet resistance CNT Layer

set cellWidth=200
loop steps=19

go atlas

set contWidthpercent=10
set divs=10
set CNTThick=0.1
set emitThick=0.4
set emitDepThick=.04
set baseDepThick=.4
set baseThick=10
set winThick=0.5
set contThick=0.1
set subThick=10
set emitMax=0
set emitDepMax=$emitMax+$emitDepThick
set baseDepMax=$emitDepMax+$baseDepThick
set baseMax=$baseDepMax+$baseThick
set baseMid=$baseMax-$baseThick/2
set subMax=$baseMax+$subThick
set winMax=$emitMax - $emitThick
set CNTMax=$winMax-$winThick
set contMax=$CNTMax-$CNTThick
set contMin=$contMax-$contThick


set winDop=1e18
set emitDop=1e18
set emitDepDop=1e18
set baseDepDop=1e17
set baseDop=1e17
set subDop=5e17

set cellWidthDiv=$cellWidth/$divs
set width3d=100e6/$cellWidth
set contWidth=25
set contWidthDiv=$contWidth/($divs)
```

```
set cellWidthHalf=$cellWidth/2

set contDiv=$contThick/($divs*10)
set CNTDiv=$CNTThick/($divs)
set winDiv=$winThick/$divs
set emitDiv=$emitThick/$divs
set emitDepDiv=$emitDepThick/$divs
set baseDepDiv=$baseDepThick/$divs
set baseDiv=$baseThick/$divs
set subDiv=$subThick/$divs


#Meshing
mesh width=$width3d
#mesh space.mult=1
#X-mesh:  Surface=500 um2 = 1/200000 cm2
x.mesh loc=-$cellWidthHalf spac=$cellWidthDiv
x.mesh loc=-$contWidth spac=$contWidthDiv
x.mesh loc=$contWidth spac=$contWidthDiv
x.mesh loc=$cellWidthHalf spac=$cellWidthDiv
#Y-Mesh
#Top of Contact
y.mesh loc=$contMin spac=$contDiv
#CNT Layer
y.mesh loc=$contMax spac=$contDiv
#Window
y.mesh loc=$CNTMax spac=$CNTDiv
y.mesh loc=$winMax spac=$winDiv
# Emitter
y.mesh loc=$emitMax spac=$emitDiv
# Depletion Region
y.mesh loc=$emitDepMax spac=$emitDepDiv
y.mesh loc=$baseDepMax spac=$baseDepDiv
# Base
y.mesh loc=$baseMax  spac=$baseDiv
# Substrate
y.mesh loc=$subMax  spac=$subDiv


# Regions
#Contact
region num=1 material=Vacuum x.min=-$contWidth x.max=$contWidth\ y.min=$contMin
y.max=$contMax
# Empty Space
region num=2 material=Vacuum x.min=-$cellWidthHalf  x.max=-$contWidth\ y.min=$contMin
y.max=$contMax
region num=3 material=Vacuum x.min=$contWidth  x.max=$cellWidthHalf\ y.min=$contMin
y.max=$contMax
# CNT Layer
region num=4 material=4H-Sic x.min=-$cellWidthHalf \ x.max=$cellWidthHalf y.min=$contMax
y.max=$CNTMax
# Window
region num=5 material=AlGaAs x.comp=0.9 x.min=-$cellWidthHalf \ x.max=$cellWidthHalf
y.min=$CNTMax y.max=$winMax
# Emitter
```

```
region num=6 material=GaAs x.min=-$cellWidthHalf x.max=$cellWidthHalf\ y.min=$winMax
y.max=$emitMax
# Emitter Depletion Region
region num=7 material=GaAs x.min=-$cellWidthHalf x.max=$cellWidthHalf\ y.min=$emitMax
y.max=$emitDepMax
# Base Depletion Region
region num=8 material=GaAs x.min=-$cellWidthHalf x.max=$cellWidthHalf\ y.min=$emitDepMax
y.max=$baseDepMax
# Base
region num=9 material=GaAs x.min=-$cellWidthHalf x.max=$cellWidthHalf\ y.min=$baseDepMax
y.max=$baseMax
# Substrate
region num=10 material=GaAs x.min=-$cellWidthHalf \ x.max=$cellWidthHalf y.min=$baseMax
y.max=$subMax



#Electrodes
electrode name=anode material=Gold x.min=-$contWidth x.max=$contWidth\ y.min=$contMin
y.max=$contMax
electrode name=cathode x.min=-$cellWidthHalf x.max=$cellWidthHalf\ y.min=$subMax y.max=$subMax

#Doping

# Window
doping uniform region=5 p.type conc=$winDop
# Emitter
doping uniform region=6 p.type conc=$emitDop
#Emitter Depletion Region
doping uniform region=7 p.type conc=$emitDepDop
#BaseDepletion Region
doping uniform region=8 n.type conc=$baseDepDop
# Base
doping uniform region=9 n.type conc=$baseDop
# Substrate
doping uniform region=10 n.type conc=$subDop

#Material Properties
material TAUN=1e-7  TAUP=1e-7  COPT=1.5e-10  AUGN=8.3e-32  AUGP=1.8e-31

#Vacuum
material material=Vacuum real.index=3.3  imag.index=0 AFFINITY=3.96

#GaAs
material material=GaAs EG300=1.42   PERMITTIVITY=13.1   AFFINITY=4.07
material material=GaAs   NC300=4.7e17  NV300=7e18
material material=GaAs   sopra=Gaas.nk

# AlGaAs
material material=AlGaAs EG300=1.5487 PERMITTIVITY=12.616 AFFINITY=3.96
material material=AlGaAs NC300=1.39e18 NV300=9.78e18 COPT=1.8e-10\ TAUN0=4.5e-9 TAUP0=2e-
8
material material=AlGaAs sopra=Algaas9.nk

# Material Properties
```

```
#CNT material properties
material material=4H-SiC  EG300=0.026  PERMITTIVITY=5.4 AFFINITY=5.8
material material=4H-SiC  NC300=3e17  NV300=3e17
material material=4H-SiC  NC.F=0  NV.F=0
material material=4H-SiC  MUN= 8138.02  MUP=8138.02
# Recombination Parameters
material material=4H-SiC  taun=0  taup=0  etrap=0
material material=4H-SiC  augn=0  augp=0
material material=4H-SiC  augkn=0  augkp=0
material material=4H-SiC  kaugcn=0  kaugcp=0
material material=4H-SiC  kaugdn=0  kaugdp=0
material material=4H-SiC  copt=0
#Optical Parameters
material material=4H-SiC  real.index=3.3  imag.index=0

#Gold
material material=Gold real.index=1.2 imag.index=1000


#Models
models conmob fldmob
models consrh

output con.band val.band

#Light Beams
#Use altered spectrum to account for CNT optical properties
beam num=1 power.file=CNT_spectrum.txt wavel.start=0.21  wavel.end=4\ wavel.num=50


#Solving
log outfile=CNT_Thermal_cell.log
solve init
method gummel  maxtraps=10  itlimit=25
solve B1=1.0
solve vanode=0  name=anode  vstep=0.1  vfinal=0.8
solve vanode=0.8  name=anode  vstep=0.01  vfinal=1.05

extract init infile="CNT_Thermal_cell.log"
extract name="opt_int" max(beam."1")
extract name="Isc" y.val from curve(V."anode", I."cathode")  where\ x.val=0
extract name="Voc" x.val from curve(V."anode", I."cathode")  where\ y.val=0
extract name="Pm" max(curve(V."anode",(V."anode"*I."cathode")))
extract name="Vm" x.val from curve(V."anode",(V."anode"*I."cathode"))\ where y.val=$"Pm"
extract name="Im" $"Pm"/$"Vm"
extract name="FF" $"Pm"/($"Isc"*$"Voc")
extract name="eff" (abs($"Pm")/$opt_int)

set cellWidth=$cellWidth + 100

l.end

# Begin loop with 76 ohm sheet resistance CNT Layer

set cellWidth=200
```

```
loop steps=19

go atlas

set contWidthpercent=10
set divs=10
set CNTThick=0.1
set emitThick=0.4
set emitDepThick=.04
set baseDepThick=.4
set baseThick=10
set winThick=0.5
set contThick=0.1
set subThick=10
set emitMax=0
set emitDepMax=$emitMax+$emitDepThick
set baseDepMax=$emitDepMax+$baseDepThick
set baseMax=$baseDepMax+$baseThick
set baseMid=$baseMax-$baseThick/2
set subMax=$baseMax+$subThick
set winMax=$emitMax - $emitThick
set CNTMax=$winMax-$winThick
set contMax=$CNTMax-$CNTThick
set contMin=$contMax-$contThick


set winDop=1e18
set emitDop=1e18
set emitDepDop=1e18
set baseDepDop=1e17
set baseDop=1e17
set subDop=5e17

set cellWidthDiv=$cellWidth/$divs
set width3d=100e6/$cellWidth
set contWidth=25
set contWidthDiv=$contWidth/($divs)
set cellWidthHalf=$cellWidth/2

set contDiv=$contThick/($divs*10)
set CNTDiv=$CNTThick/($divs)
set winDiv=$winThick/$divs
set emitDiv=$emitThick/$divs
set emitDepDiv=$emitDepThick/$divs
set baseDepDiv=$baseDepThick/$divs
set baseDiv=$baseThick/$divs
set subDiv=$subThick/$divs


#Meshing
mesh width=$width3d
#mesh space.mult=1
#X-mesh:  Surface=500 um2 = 1/200000 cm2
x.mesh loc=-$cellWidthHalf spac=$cellWidthDiv
x.mesh loc=-$contWidth spac=$contWidthDiv
```

```
x.mesh loc=$contWidth spac=$contWidthDiv
x.mesh loc=$cellWidthHalf spac=$cellWidthDiv
#Y-Mesh
#Top of Contact
y.mesh loc=$contMin spac=$contDiv
#CNT Layer
y.mesh loc=$contMax spac=$contDiv
#Window
y.mesh loc=$CNTMax spac=$CNTDiv
y.mesh loc=$winMax spac=$winDiv
# Emitter
y.mesh loc=$emitMax spac=$emitDiv
# Depletion Region
y.mesh loc=$emitDepMax spac=$emitDepDiv
y.mesh loc=$baseDepMax spac=$baseDepDiv
# Base
y.mesh loc=$baseMax  spac=$baseDiv
# Substrate
y.mesh loc=$subMax  spac=$subDiv


# Regions
#Contact
region num=1 material=Vacuum x.min=-$contWidth x.max=$contWidth\  y.min=$contMin
y.max=$contMax
# Empty Space
region num=2 material=Vacuum x.min=-$cellWidthHalf x.max=-$contWidth\ y.min=$contMin
y.max=$contMax
region num=3 material=Vacuum x.min=$contWidth  x.max=$cellWidthHalf\ y.min=$contMin
y.max=$contMax
# CNT Layer
region num=4 material=4H-Sic x.min=-$cellWidthHalf \ x.max=$cellWidthHalf y.min=$contMax
y.max=$CNTMax
# Window
region num=5 material=AlGaAs x.comp=0.9 x.min=-$cellWidthHalf \ x.max=$cellWidthHalf
y.min=$CNTMax y.max=$winMax
# Emitter
region num=6 material=GaAs x.min=-$cellWidthHalf  x.max=$cellWidthHalf\ y.min=$winMax
y.max=$emitMax
# Emitter Depletion Region
region num=7 material=GaAs x.min=-$cellWidthHalf  x.max=$cellWidthHalf\ y.min=$emitMax
y.max=$emitDepMax
# Base Depletion Region
region num=8 material=GaAs x.min=-$cellWidthHalf  x.max=$cellWidthHalf\ y.min=$emitDepMax
y.max=$baseDepMax
# Base
region num=9 material=GaAs x.min=-$cellWidthHalf  x.max=$cellWidthHalf\ y.min=$baseDepMax
y.max=$baseMax
# Substrate
region num=10 material=GaAs x.min=-$cellWidthHalf \ x.max=$cellWidthHalf y.min=$baseMax
y.max=$subMax



#Electrodes
```

```
electrode name=anode material=Gold x.min=-$contWidth  x.max=$contWidth\ y.min=$contMin
y.max=$contMax
electrode name=cathode x.min=-$cellWidthHalf  x.max=$cellWidthHalf\ y.min=$subMax
y.max=$subMax


#Doping

# Window
doping uniform region=5 p.type conc=$winDop
# Emitter
doping uniform region=6 p.type conc=$emitDop
#Emitter Depletion Region
doping uniform region=7 p.type conc=$emitDepDop
#BaseDepletion Region
doping uniform region=8 n.type conc=$baseDepDop
# Base
doping uniform region=9 n.type conc=$baseDop
# Substrate
doping uniform region=10 n.type conc=$subDop

#Material Properties
material TAUN=1e-7  TAUP=1e-7  COPT=1.5e-10  AUGN=8.3e-32  AUGP=1.8e-31

#Vacuum
material material=Vacuum real.index=3.3  imag.index=0  AFFINITY=3.96

#GaAs
material material=GaAs EG300=1.42   PERMITTIVITY=13.1   AFFINITY=4.07
material material=GaAs   NC300=4.7e17  NV300=7e18
material material=GaAs   sopra=Gaas.nk

# AlGaAs
material material=AlGaAs EG300=1.5487 PERMITTIVITY=12.616 AFFINITY=3.96
material material=AlGaAs NC300=1.39e18 NV300=9.78e18  COPT=1.8e-10\ TAUN0=4.5e-9
TAUP0=2e-8
material material=AlGaAs sopra=Algaas9.nk


#CNT material properties
material material=4H-SiC  EG300=0.026  PERMITTIVITY=5.4  AFFINITY=5.8
material material=4H-SiC  NC300=3e17  NV300=3e17
material material=4H-SiC  NC.F=0  NV.F=0
material material=4H-SiC  MUN=13889  MUP=13889
# Recombination Parameters
material material=4H-SiC  taun=0  taup=0  etrap=0
material material=4H-SiC  augn=0  augp=0
material material=4H-SiC  augkn=0  augkp=0
material material=4H-SiC  kaugcn=0  kaugcp=0
material material=4H-SiC  kaugdn=0  kaugdp=0
material material=4H-SiC  copt=0
#Optical Parameters
material material=4H-SiC  real.index=3.3  imag.index=0

#Gold
```

```
material material=Gold real.index=1.2 imag.index=1000


#Models
models conmob fldmob
models consrh

output con.band val.band

#Light Beams
#Use altered light beam to account for CNT optical properties
beam num=1 power.file=CNT_spectrum2.txt wavel.start=0.21 wavel.end=4\ wavel.num=50



#Solving
log outfile=CNT_Thermal_cell.log
solve init
method gummel  maxtraps=10  itlimit=25
solve B1=1.0
solve vanode=0  name=anode  vstep=0.1  vfinal=0.8
solve vanode=0.8  name=anode  vstep=0.01  vfinal=1.05

extract init infile="CNT_Thermal_cell.log"
extract name="opt_int" max(beam."1")
extract name="Isc" y.val from curve(V."anode", I."cathode")  where\ x.val=0
extract name="Voc" x.val from curve(V."anode", I."cathode")  where\ y.val=0
extract name="Pm" max(curve(V."anode",(V."anode"*I."cathode")))
extract name="Vm" x.val from curve(V."anode",(V."anode"*I."cathode"))\ where y.val=$"Pm"
extract name="Im" $"Pm"/$"Vm"
extract name="FF" $"Pm"/($"Isc"*$"Voc")
extract name="eff" (abs($"Pm")/$opt_int)

set cellWidth=$cellWidth + 100
l.end
```

LIST OF REFERENCES

[1] G. Xiao, Y. Tao; J. Lu; Z. Zhang, "Highly transparent and conductive carbon nanotube coatings deposited on flexible polymer substrate by solution method," *Proc. 3rd International Nanoelectronics Conference (INEC)*, pp.208–209, 3–8 Jan. 2010.

[2] J. Guo, "Carbon Nanotube Electronics, Modeling, Physics, and Applications," Doctoral Dissertation, Purdue University, 2004.

[3] B. Zeghbroeck, *Principles of Electronic Devices*, http://ecee.colorado.edu (accessed March 4, 2012).

[4] A. Bates, "Novel Optimization Techniques for Multijunction Solar Cell Design USING SILVACO ATLAS," Master's Thesis, Naval Postgraduate School, 2004.

[5] S. Michael, EC3230 Lecture Notes, Naval Postgraduate School, Winter 2004 (unpublished).

[6] S. Michael, "The Design and Optimization of Advanced Multijunction Solar Cells," Presented at the 35th *IEEE PV Specialists Conference*, Vancouver, Canada, 2004.

[7] S. Iijima, "Helical Microtubules of Graphitic Carbon," *Nature*, vol. 354, pp. 56−58, 1991.

[8] N. Srivastava, R. V. Joshi, and K. Banerjee, "Carbon Nanotube Interconnects: Implications for Performance, Power Dissipation and Thermal Management," *Electron Devices Meeting. IEDM Technical Digest*, pp. 249−252, 2005.

[9] M. S. Dresselhaus, G. Dresselhaus, and R. Saito, "Physics of Carbon Nanotubes," *Carbon*, vol. 33, no. 7, pp. 883−891, 1995.

[10] A. Alam, M. Chowalla, N. Pimparkar, "Device Optimization for Organic Photovoltaics with CNT Networks as Transparent Electode," *Proc. 33rd IEEE, Photovoltaic Specialists Conference*, pp.1–4, 11–16 May 2008.

[11] Renewable Resource Data Center (RReDC). "Solar Spectra: Air Mass Zero," http://rredc.nrel.gov/solar/spectra/am0/ (accessed April 17, 2012).

[12] J. Brunton, "TCAD Analysis of Heating and Maximum Current Density in Carbon Nanofiber Interconnects," Master's Thesis, Naval Postgraduate School, 2011.

[13] A. Crespin, “A Novel Approach to Modeling the Effects of Radiation in Gallium-Arsenide Solar Cells Using Silvaco's Atlas Software,” Master’s Thesis, Naval Postgraduate School, 2004.

INITIAL DISTRIBUTION LIST

1. Defense Technical Information Center
   Ft. Belvoir, Virginia

2. Dudley Knox Library
   Naval Postgraduate School
   Monterey, California

3. Dr. Clark Robertson, Chairman
   Department of Electrical and Computer Engineering
   Naval Postgraduate School
   Monterey, California

4. Dr. Sherif Michael, Professor
   Department of Electrical and Computer Engineering
   Naval Postgraduate School
   Monterey, California

5. Dr. Sebastian Osswald, Professor
   Department of Physics
   Naval Postgraduate School
   Monterey, California

6. ENS Adam Garfrerick
   Florence, Alabama